Aeolian–fluvial interaction within a fault-controlled basin: Late Cretaceous Chaling Basin, South China

Xiaocan Yu[a,*], Chunlian Wang[b,*], Gabriel Bertolini[c], Claiton Marlon dos Santos Scherer[c], Adriano Domingos dos Reis[d], Nigel P. Mountney[e]

[a]Institute of Geology, Chinese Academy of Geological Sciences, Beijing 100037, China

[b]MNR Key Laboratory of Metallogeny and Mineral Assessment, Institute of Mineral Resources, Chinese Academy of Geological Sciences, Beijing 100037, China

[c]Instituto de Geociências, Universidade Federal do Rio Grande do Sul, Porto Alegre 90040-060, Brazil

[d]Instituto de Geociências, Universidade de São Paulo, São Paulo 05508-080, Brazil

[e]Fluvial, Eolian & Shallow-Marine Research Group, School of Earth and Environment, University of Leeds, LS2 9JT, Leeds, UK

*Corresponding author: xiaocany1988@163.com; wangchunlian321@163.com

Abstract: The Upper Cretaceous Daijiaping Formation of the Chaling Basin, southeast China, is a mixed aeolian–fluvial succession accumulated in an erg-margin setting. The roles of climate and tectonics in governing the temporal and spatial arrangement of aeolian and fluvial strata are investigated using lithofacies and architectural-element analyses of outcrops in the eastern part of the basin. Architectural elements of aeolian origin record the preserved expression of dunes, sandsheets, damp and wet interdunes, and sand pods. Architectural elements of alluvial origin record channelized bedload streams and cobble-sand sheetflow units. Distinctive deflation lags and desert pavements are also recognized. The alternating nature of deposition via aeolian and

aqueous processes is marked by a series of sand-drift surfaces that form a record of repeated shifts from aeolian to water-lain depositional conditions. Ephemeral water influx to the desert-margin system likely occurred in response to exceptional rainfall caused by monsoonal water discharge and meltwaters from glaciated mountain ranges that bordered the basin. The vertical arrangements of alternating facies associations define stacked wetting-upward cycles, each 0.4–14.2 m thick. Each cycle commences with simple or compound crescentic dune deposits, else with aeolian sandsheet deposits. These are overlain by bedload stream or conglomerate sheetflow deposits. The vertical stacking of these different architectural elements records the contraction and expansion of erg-margin systems in response to climate-controlled variations in the groundwater level, sand availability for aeolian transport, and fluvial and aeolian sediment transport capacity. The stratigraphic evolution was controlled by exceptional rainfall events at the basin margin, consequent floods into the dune-field margin and associated fluctuations in the water-table level. Orogenic uplift, a subtropical high-pressure system, and variable groundwater level controlled by a monsoon climate and ongoing tectonic subsidence resulted in the development of extensive aeolian desert depositional systems in the South China hinterland during the Late Cretaceous.

Keywords: Daijiaping Formation, wind-water interaction, erg-margin, interdune, water table, bounding surface

1. Introduction

Dryland depositional systems are commonly characterized by diverse types of aeolian–fluvial interaction (Al-Masrahy and Mountney, 2015). Numerous prior studies

have documented types of interplay between aeolian and fluvial processes in both modern (e.g. Langford, 1989; Stanistreet and Stollhofen, 2002; Al-Farraj and Harvey, 2004) and ancient (e.g. Glennie, 1970; Langford and Chan, 1989; Veiga et al., 2002; Scherer and Lavina, 2005; Rodríguez-López et al., 2010; Reis et al., 2019; Jiao et al., 2020; Priddy and Clarke, 2020; Yu et al., 2020; Lacotte and Mountney, 2022) dryland sedimentary systems and their preserved successions. In the outer marginal regions of aeolian dune fields (henceforth erg margins), the combined effects of allogenic processes (i.e. tectonism, climate change, eustasy, water-table level) commonly generate vertical sedimentary successions that are characterized by cyclically alternating packages of strata of mixed aeolian and fluvial origin (e.g. Clemmensen et al., 1989; Mountney et al., 1999; Scherer and Lavina, 2005; Rodríguez-López et al., 2012). Recent studies have demonstrated how heavy monsoon rains were responsible for generating widespread soft-sediment deformation of aeolian dune strata in desert margin regions in the Late Cretaceous Xinjiang and Liyou basins (S China) (Rodríguez-López and Wu, 2020; Yu et al., 2021a). Slow but ongoing tectonic basin subsidence is the primary mechanism responsible for generating the accommodation required for long-term preservation of the accumulating succession. Superimposed shorter-term fluctuations of water-table level induced by climate changes may determine alternations in aeolian and alluvial processes, and resultant sedimentary facies evolution in erg-margin sedimentary systems (Cosgrove et al., 2022). Ultimately, spatial and temporal variations of ancient aeolian–fluvial successions record the combined effects of both external (i.e. allogenic) and intrinsic (i.e. autogenic) sedimentary processes.

Determining the respective roles of basin subsidence, water-table fluctuations, climate change and intrinsic sedimentary processes is challenging because of the overlapping nature of these controls and their convolved signature in the preserved sedimentary record. Detailed facies analysis and mapping is used to constrain lateral and vertical stratigraphic changes of sedimentary facies units. This approach is applied to determine how the various controls operated to give rise to the preserved erg-margin stratigraphic expression.

The aim of this study is to determine how allogenic and autogenic factors interact to govern the resultant palaeogeographic and stratigraphic evolution of sedimentary successions of mixed aeolian–fluvial origin developed in erg-margin settings. This aim is achieved through examination of the Upper Cretaceous Daijiaping Formation, which is well exposed in the fault-bounded Chaling Basin, China. The specific research objectives are as follows: (i) to describe the sedimentary architecture of the ephemeral fluvial and aeolian Daijiaping Formation; (ii) to characterize the sedimentary expression of the temporal and spatial interactions between aeolian and ephemeral fluvial processes by developing and presenting a genetic facies model; (iii) to explain the origin of ephemeral water flows into the erg-margin depositional system and to demonstrate how such flows episodically overwhelmed and reworked aeolian deposits; (iv) to evaluate how the water table varied in an actively subsiding fault-bounded basin and to explain its role in governing resultant aeolian stratigraphy; and (v) to compare this aeolian system with counterparts known form other similar settings. The outcomes of this study enhance models to explain the paleoclimatic and paleogeographic

89 evolution of East Asia during the Late Cretaceous.

90 **2. Geological setting**

91 The South China Block is characterized by an extensional Basin-and-Range
92 province, covering an area of more than 260,000 km^2 (Shu et al., 2009). It is separated
93 by the Qinling–Dabie orogen to the north from the North China Craton (Li et al., 2013).
94 It is connected to the Songpan–Ganzi Block to the west and to the Philippine Sea Plate
95 to the east (Fig. 1A). The block was created by the Early Neo-Proterozoic amalgamation
96 of the Cathaysia Block and Yangtze Block along the Jiangnan orogenic belt (e.g. Chen
97 et al., 1991; Zhao and Cawood, 1999; Zhao et al., 2011) (Fig. 1B). During the
98 Phanerozoic, the South China Block was influenced by a series of complex tectonic
99 events, including the Caledonian, Indosinian and Yanshanian orogenies (e.g. Charvet et
100 al., 1996; Zhou et al., 2006; Wang et al., 2007; Shu et al., 2008). Extension occurred
101 during the Cretaceous, associated with paleo-Pacific plate subduction (Li et al., 2019
102 and references therein). This generated numerous extensional basins (Shu et al., 2009;
103 Li et al., 2014a, b). The Cretaceous Chaling Basin is located in the north-western part
104 of the Cathaysian Block (Fig. 1B). This basin is developed upon a basement comprising
105 a Neoproterozoic to Ordovician metamorphic series, a Devonian to Lower Triassic
106 marine sedimentary rock series, and an Upper Triassic to Jurassic continental
107 sedimentary rock series (BGMRH, 1984).

108 The Upper Cretaceous in the Chaling Basin comprises the Shenhuangshan
109 Formation, the Daijiaping Formation and the Dongtang Formation, from bottom to top
110 (Fig. 1C, Table 1). The Daijiaping Formation is separated from the underlying

Shenhuangshan Formation and from the overlying Dongtang Formation by two paraconformities (Chu, 1978).

The Shenhuangshan Formation consists of red siltstones and mudstones with conglomerates at the base. Collectively, these lithotypes are representative of fluvial and lacustrine deposits (Duan et al., 1978; BGMRH, 1984). Based on the occurrence of charophyta (e.g. *Aclistochara* sp., *Obtusochara* sp.), ostracods (e.g. *Limnocypridea* sp., *Cypridea* sp., *Eucypris* sp.) and sporopollen assemblages (e.g. *Exesipollenite*s, *Schizaeoisporites*, *Pagiophyllum pollenites*), a Late Cretaceous age is demonstrated (BGMRH, 1984; Zhao, 1985). Zhao et al. (1998) proposed a K-Ar isotopic age of basalt in the Shenhuangshan Formation of 81 Ma, implying a Late Cretaceous age.

The Daijiaping Formation consists mainly of fine-grained, red sandstones and coarse sandy conglomerates of mixed aeolian and alluvial origin (Liu, 2018) (Fig. 2, Table 2). The uppermost beds within the Daijiaping Formation comprise interbedded sandstones and mudstones. Liu (2018) proposed that the succession represents an aeolian-dominated desert depositional system, but no prior attempt has been made to produce a detailed description of the nature of aeolian–fluvial interactions recorded by the succession; no prior consideration has been made of the stratigraphic evolution of this unit. The presence of dinosaur eggs (*Oolithes elongatus Young*), ostracods (e.g. *Mongolianella* sp., *Eucypris muricata*, *Talicypridea amoena*), charophyta (e.g. *Latochara brevis*, *Amblyochara* sp., *Sphaerochara brevis*), and sporopollen assemblages (e.g. *Schizaeoisporites* sp., *Pinus* sp., *Castanopsis* sp.) indicates a Late Cretaceous age (BGMRH, 1984; Zhao, 1985). The unit developed in a wider

paleogeographic context of intense aridification in eastern China, with associated intense rainfalls due to monsoon climatic seasonal changes (Chen et al., 2009; Farnsworth et al., 2019; Rodríguez-López and Wu, 2020; Yu et al., 2021a). The preserved stratigraphic record of interaction between aeolian and fluvial processes in the Daijiaping Formation demonstrates climatic and tectonic controls on aeolian–fluvial sedimentation.

The Dongtang Formation is mainly composed of red sandstones, siltstones and mudstones with sandy conglomerates, all attributed to fluvial environments (Duan et al., 1978; BGMRH, 1984). The succession contains Late Cretaceous ostracods (e.g. *Candona declivis*, *Talicypridea amoena*, *Cypridea cavernosa*), charophyta (e.g. *Maedlerisphaera minuscula*, *M.teretis*) and dinosaur eggs (*Elongatoolithus* sp.) (BGMRH, 1984).

Xi et al. (2019) proposed that the Shenhuangshan, Daijiaping and Dongtang formations are Cenomanian–Campanian, Campanian–Maastrichtian and Maastrichtian in age, respectively, according to the comprehensive analysis of biostratigraphy, chronostratigraphy and magnetostratigraphy of the Cretaceous regional stratigraphy.

3. Methodology

The data reported in this work were acquired from the examination of thirteen stratigraphic sections of the Daijiaping Formation in the Chaling Basin, China. Analysis of the depositional architecture of the continental fluvial–aeolian successions was conducted in September 2019 and November 2020. The sedimentological descriptions of field outcrops included analyses of lithofacies and facies associations and

identification and classification of bounding surfaces according to Brookfield (1977), Langford and Chan (1988), Clemmensen and Tirsgaard (1990), Kocurek (1996), Mountney (2006) and Rodríguez-López et al. (2010, 2013). Thirteen sedimentary graphic logs were measured to record the vertical stratigraphic succession of the Daijiaping Formation. Three architectural panels were constructed from photomontages and visual drawings in which lithofacies associations, sedimentary structures and stratification types were delineated.

The dip azimuths of large-scale aeolian cross-bedded dune foresets, oriented and imbricated clasts in gravel deposits, and foresets of cross-bedded sets of aqueous origin were measured to reconstruct the paleocurrents (n=138). These data were corrected to remove post-Cretaceous crustal rotation on the basis of paleomagnetic data (Sun et al., 2006), before plotted on rose diagrams. Twenty-eight thin sections were examined under a polarized light microscope to identify the grain size and the grain fabrics of the lithofacies. These procedures enabled the processes of sedimentation to be determined.

4. Lithofacies and facies associations

The Daijiaping Formation is dominated by coarse conglomerates at the basin margin and by relatively fine sediments in its central part. Fourteen lithofacies were identified based on the lithological textures and sedimentary structures present in the outcropping sections. Nine facies associations were defined in terms of the sedimentary processes. Tables 2 and 3 summarize the lithofacies and facies associations, respectively.

4.1. FA-1: Cobble to sand bedload streamflow deposits

Description. This facies association comprises matrix- and clast-supported

177 conglomerates (lithofacies Gmd, Gmp and Gct) and pebbly sandstones (Spm) with
178 minor planar cross-stratified sandstones (Spx) (Fig. 3). The conglomerates occur as
179 sheet-like bodies, bounded by erosive bases. Matrix- to clast-supported, disorganized
180 to poorly organized conglomerates (Gmd) comprise cobble to pebble clasts and granule
181 to sand matrices (Fig. 3A, B). Some elongate gravel clasts are imbricated. Clast-
182 supported, trough or planar cross-bedded conglomerates (Gct) comprise cobble to
183 pebble clasts and granule to sand matrix (Fig. 3C, D). Imbricated clasts and normal
184 grading are distinctive features of this lithofacies. Facies Gmp consists of fine pebble
185 to granule clasts in a sand matrix (Fig. 3E, F). The moderately to well-sorted gravel
186 clasts are weakly imbricated or crudely stratified. The sandstones are chiefly massive
187 (Spm) (Fig. 3D, E). Some sandstone units are crudely planar cross-stratified (Spx) (Fig.
188 3F). These sandstones are interbedded with the above conglomerates and together these
189 deposits form fining-upward units (Fig. 3D–F). The tabular unit is dm- to m-thick and
190 extends laterally for several meters to tens of meters.

191 Interpretation. The tabular conglomeratic bodies with channelized erosional bases,
192 interlayered with massive or planar cross-stratified sandstones, suggest characteristics
193 of bedload streamflow deposits (Todd, 1989; Blair, 1999). The sheet-like and
194 disorganized to poorly organized conglomerates indicate deposition of gravel sheets
195 emplaced by high-magnitude flood flows (Todd, 1989; Nemec and Postma, 1993). The
196 presence of trough cross-bedded conglomerates implies migration of gravel bars with
197 well-developed slipfaces (Blair, 1999). The normally graded units composed of
198 conglomerates and sandstones are indicative of sedimentation during waning floods

(Nemec and Postma, 1993). The deposits of successive streams are represented by stacked fining-upward units bounded by erosive bases (Todd, 1989).

4.2. FA-2: Cobble to sand sheetflood deposits

Description. This facies association comprises clast-supported planar or horizontal to low-angle cross-bedded conglomerates (Gch) and pebbly sandstones (Spm) (Fig. 4). Facies Gch is characterized by an alternation of cobble and pebble conglomerate beds or coarse pebble and sandy fine pebble conglomerate beds. These rhythmical beds show well-developed couplets. Laterally variable pinch-out of the couplet beds is observed in this lithofacies. Amalgamated conglomerate beds (meters to tens of meters thick) commonly contain massive sandstone lenses (Fig. 4). The pebbly sandstones (Spm) are interbedded with lithofacies Gch showing fining-upward units (Fig. 4F). Units of this facies association are meters to tens of meters thick and several tens of meters wide, forming sheet-like conglomeratic bodies. The base of these conglomerate beds shows flat surfaces or low-relief scoured features of the underlying sediments.

Interpretation. The characteristic alternating conglomerate beds bounded by flat or low-relief bases are interpreted as sediment-charged, upper-flow-regime sheetflood deposits under high-energy flashy flooding (Turner, 1980; Todd, 1989; Malmon et al., 2004; Wakelin-King and Webb, 2007). This process might record catastrophic flood events (Blair and McPherson, 2009). The couplets in lithofacies Gch are usually the result of breaking and downslope destruction process of supercritical standing waves by violent washout (Blair, 2000; Blair and McPherson, 2009). Multistory stacked depositional lobes are indicated by the broad and thick sheet-like bodies and the

occurrence of prominent scoured basal surfaces with only low-relief (Blair, 2000). The alternating pebbly sandstones and conglomerates formed under conditions of waning floods (Todd, 1989).

4.3. FA-3: Meandering fluvial channel deposits

Description. This facies association comprises matrix-supported conglomerates (Gmi), ripple cross-bedded sandstones (Sr), massive tabular sandstones (Sm) and lenticular or laminated silty mudstones (Fl) (Fig. 5A–C). The unit is present in the north-central part of the basin. These lithofacies types form fining-upward depositional cycles bounded by low-relief basal erosion surfaces. Each cycle is decimeters thick and extends laterally for tens of meters. The basal conglomerates (lithofacies Gmi) consist of fine pebble to granule clasts in a fine sand matrix. The pebble clasts are dominantly of purple mudstone of intraformational origin (Fig. 5C).

Interpretation. The presence of tabular deposits arranged into cycles, each with an erosive base and internally recording a fining-upward grainsize trend (i.e. normal grading), might indicate accumulation within meandering fluvial channels (Miall, 1996; Scherer et al., 2007; Ghazi and Mountney, 2009). The basal conglomerates with erosive bases represent channel lag deposits generated by erosion of the basal channel (Ghazi and Mountney, 2009). The dominance of mud intraclasts implies the localized reworking fine sediments, possibly form a nearby floodplain (Scherer et al., 2007; Ghazi and Mountney, 2009). The thin sand bodies composed of horizontal and massive sandstones with ripple cross-lamination represent deposits of relatively shallow fluvial channels under conditions of fast and intermittent sheet-like flow (Miall, 1996). The

243 cm-thick silty sediments at the top of each cycle are products of setting of fine
244 suspended loads under decreasing flow velocity (Smith et al., 1989; Bridge, 2003).

245 4.4. FA-4: Overbank flood and floodplain deposits

246 Description. This facies association comprises packages of tabular fine-grained
247 sandstones (Sm) and laminated silty mudstones (Fl) with no erosive bases (Fig. 5A, D).
248 The tabular packages are decimeter to meter thick and extend laterally for tens of meters.
249 Pale grey-green mottling, slickensides and silty aggregates are notable in the meter-
250 scale thick massive mudstone beds (Fig. 5E).

251 Interpretation. The tabular and laterally continuous packages of alternating
252 mudstones and sandstones without evident erosional features suggest deposition from
253 unconfined flows that characterize overbank regoins lateral to fluvial channels (Smith
254 et al., 1989; Miall, 1996), especially where splays are developed (Burns et al 2019;
255 Colombera and Mountney, 2022). The vertical stacking of such cycles indicates flash-
256 flood events of short duration and rapid flow deceleration in the aftermath of the
257 flooding (Miall, 1996; Bridge, 2003). The presence of red coloration, mottling and
258 slickensides in mudstones suggests oxidizing conditions and pedogenic alteration,
259 accompanied by episodic waterlogging and localized decomposition (Retallack, 1994;
260 Soares et al., 2020; Basilici et al., 2022). Pedogenic calcretes are characteristic features
261 of the paleosols (Liu, 2008). The occurrence of stacked paleosol levels indicates
262 floodplain deposits featured by episodes of sediment aggradation along with subaerial
263 exposure (Bridge, 2003; Basilici et al., 2024). The presence of meter-scale massive
264 mudstones suggests that floodplain environments could have formed during high-

magnitude flood conditions (Scherer et al., 2007).

4.5. FA-5: Deflation lags and desert pavements

Description. This facies association is characterized by discrete lags (Gc(e)) of limestone and quartzite pebbles and cobbles that extend laterally for several or tens of meters (Fig. 6). Pebble- to cobble-grade lags form horizontal and planar lineations with the thickness of one pebble or cobble. The pebbles are mostly 1–5 cm long and the cobbles have lengths of ~7–10 cm, with some individual boulders >26 cm. These lags are represented by isolated or juxtaposed arrangement along the lineation and contain pyramid-shaped pebbles and cobbles with polished surfaces and sharp facetted edges (Fig. 6B). Pebble and cobble lags are covered by aeolian sandstones (Sl(e) or St(e)) (Fig. 6).

Locally, deflation lags of limestone and quartzite pebbles and cobbles show decimeter-thick vertical stacking of tabular clast-supported conglomerates (Gc(e)) (Fig. 6C, D). They are bounded by flat top and base surfaces and display large cobbles in the upper part. Beds of tabular lithofacies Gc(e) are covered by aeolian sands that penetrated into and filled the space between the gravel below. Matrices consist of fine sand and granules.

Interpretation. These discrete and laterally persistent pebble to cobble lags are similar to deposits recognized by previous studies as deflation lag by wind (e.g. Clemmensen and Abrahamsen, 1983; Dávila and Astini, 2003; Li et al., 2006; Rodríguez-López et al., 2010). These deflation lags represent distinct ventifacts with polished surfaces and sharp edges, indicating strong abrasion under the effect of

windblown sand (e.g. Glennie, 1970; Knight, 2008). Such deflation lags are normally closely associated with aeolian deposits of desert systems. They are formed by intense wind deflation and reworking of ephemeral fluvial deposits.

The long-lasting and repeated wind deflation of ephemeral fluvial deposits to form stacked deflation lags leads to the formation of desert pavements (Dorn, 1990; Al-Farraj and Harvey, 2000). The concentration of pebbles upon such surfaces generates an armored surface that prevents further deflation of underlying sandy sediments. Desert pavements are several pebbles or cobbles thick, whereas deflation lags are characterized by a lineation with the thickness of one pebble or cobble (Dorn, 1990; Al-Farraj and Harvey, 2000).

4.6. FA-6: Aeolian sandsheet

Description. This facies association comprises well-sorted fine- to coarse-grained sandstones (Sl(e)) arranged into tabular units (Figs. 7, 8). It forms 0.08 to 9 m thick sets that extend laterally more than 50 m (the maximum extent). Sets occur intercalated with deflation lags. Internally, deposits are characterized by stacked horizontal or low-angle laminae 0.2 to 2.5 cm thick with inverse grading. Laminae are distinguished by variations in granularity and color (Figs. 7C, 9A). Facies Sl(e) occurs interbedded with aeolian cross-stratified sandstones (St(e)) (Fig. 7A) or water-lain conglomerates (Gch) (Fig. 8). Locally, thick intervals appear alone marked by the interlayer of lags of granules and wind-ripple deposits (Fig. 7D, E).

Interpretation. These tabular intervals of well-sorted fine-grained laminated sandstones represented by low-angle or horizontal to subhorizontal wind-ripple laminae

are indicative of deposition in aeolian sandsheets (Hunter, 1977; Fryberger et al., 1983, 1992). The persistent lateral extension of this facies without significant variation implies relatively steady aeolian transport and deposition. The thick intervals formed of subcritically climbing translatent strata (*sensu* Hunter, 1977) and composed by flat and discrete laminae of texturally and compositionally fine sand, granules and small pebbles accumulations are very similar to deflation lags described by Clemmensen and Abrahamsen (1983) and Rodríguez-López et al. (2010, 2012). The armoring is a consequence of the partial deflation of the bimodal deposits to leave the coarser grains at the surface. In conditions of high wind velocities, lag granules and small pebbles from adjacent water-lain gravels are incorporated into well-sorted windblown sands (Glennie, 1970; Clemmensen and Abrahamsen, 1983).

4.7. FA-7: Aeolian dune

Description. This facies association comprises light pink very fine- to fine-grained sandstones (St(e)) (Figs. 8, 10–15). These sandstones are formed by tabular bodies 0.3–6.8 m thick, arranged in trough-tangential cross-stratified sets that can be extended up to tens of meters laterally. Concave-up foresets are represented by massive or inversely graded laminae (Figs. 9B, 10), showing a unidirectional dip spread in a single set. A clear surface hierarchy (marked ‘R’, ‘S’ and ‘IS’ in Figs. 11–14) is observed in the cross-bedded sets. Continuous lag deposits of granule and small pebbles are distributed along the bounding surfaces (Fig. 11E, F). Trough cross-bedded sandstones (St(e)) bounded by relatively flat surfaces (marked ‘SDS’ and ‘FS’) are interbedded with water-lain conglomerates (Gch) (Figs. 11A, C, 12 and 13), else are completely

331 embedded in the lithofacies Gch (Figs. 12, 14). Abundant poikilotopic calcite
332 cementation is observed in the cross-bedded sandstones (Fig. 9C, D).

333 Interpretation. The large-scale cross-bedded sets with grainflow strata consisting
334 of well-sorted sandstones are interpreted as the deposits of aeolian dunes with slipfaces
335 (Hunter, 1977; Kocurek, 1991, 1996; Mountney, 2006). The different hierarchies of
336 bounding surfaces presented in these aeolian dunes are consistent with those defined by
337 Brookfield (1977) and Kocurek (1981), indicating different aeolian processes (Rubin,
338 1987; Kocurek, 1991, 1996). The subhorizontal surfaces (marked 'IS') overlain by
339 lenticular or tabular muddy sand bodies are equivalent to the interdune surfaces
340 described by Jones et al. (2016) in the Permian Santa Brígida Formation, Brazil. These
341 interdune surfaces are formed by the migration and climbing of dune and interdune
342 deposits (Kocurek, 1981, 1991). The subhorizontal concave-up surfaces (marked 'S')
343 separating aeolian cross-bedded sets are interpreted as superimposition surfaces
344 (Kocurek, 1991; Scherer, 2000). The downwind-dipping and concave-up surfaces
345 (marked 'R') occurring in the dune forests are interpreted as reactivation surfaces
346 (Kocurek, 1991; Mountney and Thompson, 2002). The formation of these reactivation
347 surfaces is the result of erosion and reworking of aeolian dune foresets owing to changes
348 in wind directions and/or bedform migration directions (Kocurek, 1981; Mountney,
349 2006). The relatively flat surfaces (marked 'SDS') that separate the overlying aeolian
350 facies from the underlying water-lain deposits are interpreted as sand-drift surfaces
351 (Clemmensen and Tirsgaard, 1990); they record aeolian deflation of fluvial deposits as
352 indicated by the occurrence of the ventifacts (Fig. 6A, B). The subhorizontal surfaces

(marked ‘FS’) atop the aeolian sandstones are erosive flood surfaces; they record an increase in the superficial runoff promoting accumulation of fluvial deposits (Langford and Chan, 1988; Scherer and Lavina, 2005; Rodríguez-López et al., 2013).

Laterally continuous granule lags on bounding surfaces demostrate deflation of the underlying bimodal aeolian deposits (Clemmensen and Abrahamsen, 1983; Kocurek and Nielson, 1986). The presence of fine pebbles in the toesets of aeolian dunes indicates the presence of wadis or similar dryland channels adjacent to the toes of aeoliansand dunes (Tanner and Hubert, 1992; Turner and Makhlouf, 2002; Rodríguez-López et al., 2010). Glennie (1970) reported aeolian dunes containing pebbles and cobbles, similar to the units observed here; these pebbles and cobbles are reworked by sliding and rolling from the banks of adjacent wadis. Similar examples of aeolian dunes containing extraformational granules, pebbles and cobbles were described by Clemmensen and Abrahamsen (1983) for Permian desert deposits in the Arran Basin of Scotland, by Turner and Makhlouf (2005) for Pliocene to Pleistocene desert systems in northeast Jordan, and by Rodríguez-López et al. (2010) for the mid-Cretaceous back-erg margin system in eastern Iberia.

The remnants of aeolian deposits that are reworked by water are interpreted as aeolian pods (*sensu* Porter, 1987). Similar aeolian pods have been reported from the erg-margin system of the Lower Jurassic Aztec Sandstone in USA (Porter, 1987), and from the Early Albian to Early Cenomanian Iberian desert system close to the Variscan Massif in eastern Iberia (Rodríguez-López et al., 2010). Clark and Rendell (1998) described the wind-water interaction occurring in the Mojave Desert in USA, where

alluvial sheet-wash processes close to a cliff led to the episodic erosion and removal of encroaching aeolian sands. The aeolian pods studied here may have formed via a similar process. The presence of poikilotopic calcite cementation, widespread in some aeolian sandstones (Worden and Burley, 2003; Henares et al., 2014; Bertolini et al., 2021), may be generated in reponse to water percolation and evaporation after flooding (Bertolini et al., 2021).

4.8. FA-8: Damp interdune

Description. This facies association is characterized by lenticular or tabular decimeter-thick intervals of structureless fine-grained sandstones (Ss) (Figs. 13–14). These units pinch out against sets of cross-bedded aeolian dunes laterally. The architectural arrangement commonly records an interfingering relationship with the toesets of the overlying aeolian dune cross-strata.

Interpretation. The occurrence of decimeter-thick lens-shaped units interlayered with aeolian dune cross-stratification suggests interdune deposits (Kocurek, 1981; Scherer and Lavina, 2005; Dias and Scherer, 2008). The lenticular bodies of massive, fine-grained sandstones define deposition in a damp interdune where the capillary fringe of the groundwater level reached the depositional surface that captured windblown dust and sand grains. The intertonguing of overlying aeolian dune toesets with interdune deposits indicates simultaneous advance of both the interdunes and the neighboring dunes (Pulvertaft, 1985; Mountney and Thompson, 2002; Jones et al., 2016). Meanwhile, high rates of cannibalization of interdune deposits during dune migration are indicated by the small thickness and the lens-shaped geometry of the units

(Mountney, 2012).

4.9. FA-9: Wet interdune

Description. This facies association comprises interbedded very fine-grained sandstones (Sm) and silty mudstones (Fl) (Fig. 15). It forms a decimeter-thick lenticular geometry and pinches out between the cross-bedded aeolian dunes. The unit passes laterally to cobble and pebble deflation lags (Fig. 15E, F). The intertonguing contact between this architectural element and the toesets of the overlying cross-strata of aeolian dunes are observed.

Interpretation. The presence of the decimeter-thick lenticular geometry consisting of interbedded sandstones and mudstones, and the intertonguing with the toesets of the overlying aeolian dune cross-strata indicates a wet overbank-interdune element that developed in areas where the interdune depressions were flooded (Kocurek, 1981; Langford and Chan, 1989; Mountney and Thompson, 2002). The occurrence of cobble to pebble deflation lags on the interdune surface may imply contemporaneous flooding by fluvial incursion and dune migration (Langford and Chan, 1989).

5. Depositional model

The combined lithofacies and architectural-element analysis allows identification of changes in the depositional systems over time. The facies successions of the Daijiaping Formation exhibit a clear spatial zonation that records an alternation of aeolian and alluvial deposits in the alluvial fan setting in the eatern part of the basin (Fig. 2). The fluvial and floodplain deposits are distributed in the north-central portion. The lower part of the Daijiaping Formation is characterized by thick conglomerates that

419 unconformably overlie the Paleozoic strata in the eastern basin (Gao, 1975; Chu, 1978).
420 The upper part of this formation is represented by silty mudstones and sandstones with
421 sandy conglomerates that are bounded at their top by a regional paraconformity (Gao,
422 1975; Chu, 1978).

423 The thick cobble to sand bedload stream deposits constitutes the basal interval of
424 the Daijiaping Formation (Fig. 2). These gravelly streamflow deposits are indicative of
425 deposition in the medial part of an alluvial fan system; the sandstone sheet-like deposits
426 are typical of the deposits of the distal portion of an alluvial fan (Blair, 1999). The
427 paleocurrents indicate an overall westward transport direction for the alluvial deposits
428 (Fig. 16A). These streamflow and sheetflow deposits, which dominantly comprise
429 cobbles to sand, are likely the accumulated deposits of high rainfall events that
430 originated in the highland that bounded the basin to the east (cf. Clemmensen et al.,
431 1989; Rodríguez-López et al., 2010). Meanwhile, a poorly confined ephemeral fluvial
432 system comprising fluvial channel and overbank flood deposits developed in the north-
433 central part of the basin. The floodplains were supplied with sediment during high-
434 magnitude flood events.

435 The water-lain sediments pass upward into interbedded aeolian and fluvial
436 deposits, accumulated units of which are bounded by sand-drift surfaces (Fig. 2). The
437 sandy sediments in the alluvial deposits were a major source for the subsequent
438 construction of the aeolian deposits.

439 These alternating aeolian and fluvial deposits indicate the occurrence of an arid to
440 semi-arid climate regime (Mountney et al., 1998). They are common in erg margins

441 subject to periodic or episodic flooding and dune accumulation. They develop in
442 response to fluctuations in sediment supply and water-table level (Langford and Chan,
443 1989; Mountney et al., 1998; Mountney and Jagger, 2004). The vertical changes in
444 sedimentary architecture of the aeolian–fluvial successions recorded repeated
445 expansion and contraction of the aeolian system.

446 During deposition of the aeolian–fluvial unit, aeolian dunes, damp and wet
447 interdunes, aeolian sandsheets, deflation lags and desert pavements represent the wind-
448 related facies associations. These occur interbedded with streamflow or sheetflow
449 deposits. The preserved aeolian dune architecture is typical of simple and compound
450 crescentic dunes without appreciable dry interdune deposits. This stratal arrangement
451 indicates a dry aeolian system where the water table lay significantly below the level of
452 the depositional surface (Fig. 16B). Elsewhere, the presence of both damp- and wet-
453 interdune deposits records oscillations in the water table developed within an overall
454 wet aeolian systems (*sensu* Kocurek and Havholm, 1993) (Fig. 16C).

455 The dune foreset dip-azimuth data recorded in the aeolian sandstones (Fig. 2)
456 suggest dominant westerlies followed by northeasterlies and minor northwest and
457 southeast winds, which agree with Late Cretaceous global circulation models and
458 paleowind pattern that existed in the middle and low latitudes of the Northern
459 Hemisphere (Jiang et al., 2008; Hagegawa et al., 2012; Yu et al., 2021b). The ephemeral
460 fluvial deposits are represented by episodic, channelized cobble to sand bedload
461 streams and sheet floods. The long-lasting wind deflation of these ephemeral fluvial
462 deposits led to the occurrence of deflation lags and desert pavements.

Overall, the fluvial–aeolian succession comprises water-lain deposits passing upward to arid to semi-arid cyclic deposits of mixed aeolian and fluvial origin. The inferred arid and semi-arid climate regime favored the development of an alluvial system generated by episodic flooding followed by intense erosion and subsequent wind accumulation. The described aeolian and fluvial sedimentary systems are typical of erg-margins settings (Mountney and Jagger, 2004; Mountney, 2006). The vertical arrangement of these sedimentary architectures is the most obviously stratigraphic expression of the contraction and expansion of erg-margin systems in response to allogenic variations of climate, with accommodation and long-term preservation of the overall accumulation enabled by tectonic subsidence.

6. Discussion

6.1. Stratigraphic model and controlling factor of aeolian–fluvial sedimentation

The aeolian–fluvial deposits in the Daijiaping Formation represent alternating aeolian and fluvial units, bounded by erosive surfaces (flood surfaces and sand-drift surfaces) that divide the sedimentary succession into different facies associations (Fig. 17). Sedimentological characteristics and the contacts between these sedimentary facies indicate that the aeolian dune, damp and wet interdune, aeolian sandsheet and fluvial deposits show episodes of flooding and aeolian accumulation.

The vertical stacking of aeolian–fluvial deposits reveals a series of ‘wetting-upward’ cycles, each 0.4–14.2 m thick. Each of these cycles is characterized by simple or compound crescentic dune or aeolian sandsheet deposits, overlain by bedload streamflow or conglomerate sheetflow deposits. The development of the bounding

surfaces occurring in these cycles is function of fluvial and aeolian sediment transport capacity, dry sand availability and relative water table (Kocurek, 1988; Kocurek and Lancaster, 1999).

The aeolian deposits in the aeolian–fluvial unit mainly consist of two types of aeolian deposits: dry and wet aeolian systems (*sensu* Kocurek and Havholm, 1993) (Fig. 17). The typical sedimentary successions of these aeolian systems record oscillations in water-table level. The dry aeolian system encompasses superimposed aeolian dune cross-sets without appreciable intervening interdunes, indicating that sedimentation developed in settings with a water table below the depositional surface and a high sediment availability and aeolian transport capacity. The wet aeolian system is characterized by damp interdune facies consisting of massive muddy sandstones and wet interdune facies composed of interbedded very fine sandstones and silty mudstones, indicating a water table close to or above the depositional surface, respectively. Aeolian accumulation commenced atop sand-drift surfaces. The limited availability of dry sand suitable for aeolian transport prevented widespread aeolian dune construction, but was sufficient for the formation and development of aeolian sandsheets (Fig. 17).

The flood surface represents an interruption in aeolian accumulation and forms when the rising groundwater level is accompanied by an increase in the surface runoff. Thus, it can aid the accumulation of streamflow deposits atop the aeolian deposits, especially given an associated decrease in downstream aeolian transport capacity. A gradual but progressive increase in the surface runoff limits sand availability for aeolian transport and ultimately favors the accumulation of streamflow deposits.

507 The aeolian deposits of the next (i.e. overlying) cycle rest above a sand-drift
508 surface with deflation down to the water-table level during periods of water table fall
509 (Fig. 17). The availability of dry sand for aeolian transport is high at the end of the fall,
510 allowing aeolian system accumulation to resume at the onset of accumulation of the
511 next cycle.

512 The occurrence of these alternating aeolian and fluvial deposits in an
513 intracontinental basin is likely associated with fault-controlled subsidence and
514 combined with episodic fluctuations in the climate regime. These factors acted to
515 influence sand availability, sediment supply, aeolian and fluvial transport capacity and
516 water-table level (Kocurek, 1988, 1999; Kocurek and Lancaster, 1999).

517 The fault-dominated basin subsidence can cause a relative water-table rise,
518 promoting the accumulation and preservation of the aeolian and fluvial sedimentary
519 succession (Scherer and Lavina, 2005; Cosgrove et al., 2022). However, the
520 interbedded aeolian and fluvial units and the development of flood surfaces and sand-
521 drift surfaces indicate that the water table rise in the Daijiaping Formation was not a
522 uniform process, and that frequent fluctuations of water-table position and sediment
523 supply resulted from climate changes (Fig. 18). Similar wetting-upward cycles in the
524 fluvio-aeolian successions driven by climate forcing are also confirmed by previous
525 studies (e.g. Clemmensen et al., 1989, 1994; Howell and Mountney, 1997; Mountney
526 et al., 1998; Veiga et al., 2002; Scherer and Lavina, 2005; Mayoral et al., 2021).

527 6.2. Causes of sudden water fluxes and subsequent mass transport

528 The presence of cobble to sand bedload stream and pebble-sand sheetflood

deposits and aeolian pods in the aeolian–fluvial succession indicates the great fluxes of ephemeral waters (Porter, 1987; Rodríguez-López et al., 2010, 2012). Large flood events can occur in an arid to semi-arid climate setting. Floodwaters can erode aeolian deposits catastrophically (Svendsen et al., 2003; Mack et al., 2008), as reported from the mid-Cretaceous back-erg margin system in the eastern Iberia of Spain (Rodríguez-López et al., 2010). This effect results in the reworking of wind-related deposits (dunes, sandsheets, deflation lags and desert pavements), as corroborated by the presence of distinct aeolian pods (Figs. 12, 15; see section 4.7 for interpretation).

Possible mechanisms responsible for sudden water influx into the Chaling desert margin system include (i) monsoonal rainfall discharge and (ii) meltwater drainage from adjacent glaciated mountain ranges.

Monsoonal water discharge in aeolian deserts can trigger associated deformation processes of aeolian dune deposits (Loope et al., 2001). These soft-sediment deformation structures associated with monsoon rainfall have been reported from the Upper Cretaceous aeolian dune deposits of South China (Rodríguez-López and Wu, 2020; Yu et al., 2021a). The East Asian annual rainfall during the Late Cretaceous occurred during the summer monsoon from June to August (Chen et al., 2009; Farnsworth et al., 2019). The Chaling desert streams fed by intense monsoon rainfall likely carried floodwaters to the erg-margin system leading to episodic erosion and reworking of aeolian deposits and the emplacement of ephemeral fluvial deposits.

Meltwater fluxes from the surrounding glaciated mountains in desert basins have been documented from the Quaternary Taklamakan desert in western China (Yang et

al., 2006) and the mid-Cretaceous Iberian desert in eastern Spain (Rodríguez-López et al., 2010). The fluvio-aeolian deposits in the Late Cretaceous Chaling desert system bear similarity to these examples with respect to the presence of interbedded aeolian and streamflow deposits, deflation lags and desert pavements. Meltwater flows from alpine glaciers of the Wanyang mountain range to the east of the Chaling Basin may have discharged the Chaling desert system leading to the input of coarse streamflow deposits and the reworking of previous aeolian deposits (Xiao et al., 2019). The Cretaceous South China is characterized by alternating episodes of shortening and extension in response to the subduction and rollback of the paleo-Pacific Plate (Li et al., 2014b, 2020). In the Late Cretaceous, a coastal mountain range with a paleoelevation of ≥ 2000 m existed along the South China margin due to the collision between the Okhotomorsk Block and the South China Block (Chen, 2000; Yang, 2013; Zhang et al., 2016, 2021; Chen et al., 2021). Meanwhile, intra-continental orogens manifest in South China as mountain ranges with high elevation and extensional fault basin (Yang, 2003; Li et al., 2014b, 2020). Combined with the clockwise rotation of the South China (Sun et al., 2006), the Wanyang mountains close the Chaling desert margin should have sufficient altitudes for orographic rains, snow showers and the accumulation of ice at subtropical latitudes (Wang et al., 1998).

Considering the geological background of the Late Cretaceous South China, the input of water influx in the Chaling Basin is a result of one or a combination of the two hypotheses: a glaciated Wanyang mountain range in conjunction with monsoonal rainfall.

6.3. Aeolian–fluvial interaction in modern and ancient sedimentary systems

Aeolian and fluvial processes in ancient and modern desert-margin settings exhibit diverse interaction types, notebly fluvial incursions into aeolian dune fields by various processes and flooding within aeolian dune fields due to the elevation of groundwater levels to the surface in response to intense precipitation and associated fluvial run off (Langford and Chan, 1989; Langford, 1989; Al-Masrahy and Mountney, 2015). The primary factors that govern the nature of flooding in modern fluvial–aeolian systems are aeolian dune morphology, the length of time during which the interdune is exposed and the water-table level (Langford, 1989). Within the fluvial–aeolian systems, sub-environments within which flood-related deposition occurs include wet interdunes, playas within interdunes and ephemeral fluvial channels and sheets. The irregular flood surfaces level dune topographic relief, whereas aeolian dunes generate positive topographic relief. Distinct types of fluvial–aeolian interactions arise in response to the variable nature of how fluvial incursions occur within aeolian dune fields. Based on the analysis of sedimentary characteristics and geometric properties of the preserved deposits of aeolian–fluvial interaction system in the Permian Culter Group, Paradox Basin, USA, a classification scheme for ancient aeolian–fluvial architectural elements is introduced to characterize sedimentary variability in three dimensions (Lacotte and Mountney, 2022). To classify and understand the nature of aeolian–fluvial interaction process that operated in the fluvial-aeolian system represented by the Daijiaping Formation, available study-cases on similar units are here compiled to draw comparisons (Table 4). Three distinct types of fluvial–aeolian interactions are

595 recognized: (1) short-term aeolian–fluvial interaction characterized by the dominance
596 of fluvial activity over small-scale aeolian activity; (2) fluvial incursions into aeolian
597 dune fields without elevated water-table levels; and (3) fluvial incursions into aeolian
598 dune fields associated with elevated groundwater levels.

599 The sedimentological record of short-term aeolian–fluvial interaction
600 characterized by the dominance of fluvial activity over small-scale aeolian activity is
601 represented by centimeter- to meter-thick sets of aeolian wind-ripple strata or cross-
602 bedding of aeolian dune origin that occur within a succession of strata that is otherwise
603 of fluvial origin. Localised aeolian reworking of fluvial deposits is the main fluvial-
604 aeolian interaction type. Accumulation and preservation of aeolian deposits is
605 controlled by the architecture of the fluvial system. The resulting change from fluvial
606 to aeolian is related to short-term shifts in aridity (semi-arid to arid climate), possibly
607 on a seasonal basis, as in the Proterozoic Mancheral Quartzite, India (Chakraborty and
608 Chaudhuti, 1993), Middle Proterozoic Eriksfjord Formation, southwest Greenland
609 (Tirsgaard and Øxnevad, 1998), the Upper Silurian Tumblagooda Sandstone, western
610 Australia (Trewin, 1993), the Siluro-Devonian Swanshaw Sandstone Formation, SW
611 Scotland (Smith et al., 2006), and the Upper Cretaceous capping sandstone,
612 Kaiparowits Basin, USA (Simpson et al., 2008).

613 The sedimentological record of fluvial incursions into aeolian dune fields without
614 elevated water-table levels is represented by deposits of aeolian dunes, aeolian
615 sandsheets, fluvial channels, sheet-like flows, and floodplains. Water-lain deposits
616 within the fluvial–aeolian system are characterized by deposits of ephemeral fluvial

617 origin that overlie erosive flood surfaces. Aeolian deflation surfaces (sand-drift surfaces)
618 are common in the resultant succession. Aeolian strata mostly comprise deposits of a
619 dry-aeolian setting, without damp, wet or fluvially flooded interdunes. Unconfined
620 sheetflood deposition, fluvial breaching of aeolian dune topography and amalgamated
621 channel-forms arising from long-lasting confined flooding are dominant in the aeolian–
622 fluvial interaction type. The alternating fluvial and aeolian deposits produce distinct
623 dry-wet cycles, each several meters to tens of meters thick, as is the case for the Upper
624 Permian Dawlish Sandstone Formation of the Wessex Basin, UK (Newell et al., 2001),
625 the Permian Brodick Beds, UK (Clemmensen and Abrahamsen, 1983; Frederiksen et
626 al., 1998), the Upper Jurassic Tianchihe Formation, Ningwu–Jingle Basin, China (Xu
627 et al., 2019), the Upper Jurassic–Lower Cretaceous Guará Formation of the Paraná
628 Basin, southern Brazil (Scherer and Lavina, 2005, 2006) and Batoví Member of the
629 Norte Basin, Uruguay (Amarante et al., 2019), the Lower Cretaceous Avilé Member of
630 the Neuquén Basin, Argentina (Veiga et al., 2002), and Lower Cretaceous São Sebastião
631 Formation of the Jatobá Basin, Brazil (Ferronatto et al., 2019). The vertical variations
632 from fluvial to aeolian deposits record cyclical climatic changes from relatively humid
633 to semi-arid to arid conditions.

634 The sedimentological record of fluvial incursions into aeolian dune fields
635 associated with elevated groundwater levels is mainly represented by the deposits of
636 aeolian dunes, aeolian sandsheets, dry, damp and wet interdunes, braided and ephemeral
637 fluvial channels, and unconfined fluvial sheet-like flows. Sheet-like water-lain deposits
638 within these fluvial–aeolian successions are characterized by wet interdunes, playas

639 with interdunes and ephemeral fluvial deposits bounded by flood surfaces and sand-
640 drift surfaces. The geometric properties of the sedimentary architectural elements are
641 diverse, as defined by Lacotte and Mountney (2022) as seven types of aeolian–fluvial
642 interaction. The occurrence of variably dry to wet interdune architectural elements
643 indicates a changing water-table level as sedimentation was onging. Vertical drying-
644 wetting cycles, each up to tens of meters thick, are common, as in the Pennsylvanian
645 Piauí Formation of the Parnaíba Basin, Brazil (Vieira and Scherer, 2017; Kifumbi et al.,
646 2022), the Permian Cutler Group of the Paradox Basin, USA (Langford and Chan, 1989;
647 Mountney and Jagger, 2004; Jordan and Mountney, 2010; Cain and Mountney, 2011),
648 the Permian De La Cuesta Formation of the Paganzo Basin, NW Argentina (Spalletti et
649 al., 2010), the Permian Upper Rotliegend Group, North Sea (Ellis, 1993; Sweet, 1999),
650 the Triassic Helsby Sandstone Formation and Ormskirk Sandstone, UK (Mountney and
651 Thompson, 2002; Cowan, 1993; Herries and Cowan, 1997), the Lower Jurassic Kayenta
652 and Navajo Sandstone formations of the Colorado Plateau, USA (Herries, 1993; Hassan
653 et al., 2018; Priddy and Clarke, 2020), the Upper Jurassic Quebrada del Sapo Formation
654 of the Neuquén Basin, Argentina (Veiga and Spalletti, 2007; Spalletti and Veiga, 2007),
655 the Lower Cretaceous Twyfelfontein Formation of the Huab Basin, northwest Namibia
656 (Mountney et al., 1998, 1999), the Upper Cretaceous Barun Goyot Formation of the
657 Gobi Basin, Mongolia (Gradzinski and Jerzykiewicz, 1974), and the Upper Cretaceous
658 Daijiaping Formation of the Chaling Basin, China. Basin- and Larger-scale fluvial–
659 aeolian sedimentary cycles of basin-wide exntent record region-wide, longer-term
660 climatic variations. Smaller-scale fluvial–aeolian sedimentary cycles mostly record

individual localized fluvial flood events into the marings of aeolian dune fields (Almasrahy and Mountney, 2015; Lacotte and Mountney, 2022).

Overall, the fluvial–aeolian interaction styles proposed here are expressed as preserved depositional cycles that can be related to episodes of heightened aridity within an evolving basin. The changes in aridity are particularly important as controls on the aeolian deposition (e.g. dry- to wet-interdunes). Although climate is considered the dominant control on the style of fluvial and aeolian deposition, tectonic basin subsidence generates the long-term accommodation necessary for preservation of successive cycles. Variations in the background rates of subsidence, for example as might be induced by episodic movement of basin-bounding faults, may induce fluctuations in the water-table level (Mountney, 2004; Lancaster and Mountney, 2021).

The accumulation and preservation of sedimentary cycles associated with these aeolian–fluvial depositional systems indicates that an arid climate prevailed, periodically recharged by surface flooding and groundwater. Within each cycle, the arid episode is characterized by the formation of extensive aeolian deflation surfaces and subsequently by aeolian-dune construction and accumulation. Short-term arid episodes preserved only thin accumulations of aeolian deposits. During humid episode, fluvial flooding into the margins of aeolian dune fields occurred. Such flooding might have occasionally extended into dune-field interiors, resulting in the formation of distinctive flood surfaces (*sensu* Langford and Chan, 1988). This is recorded by the presence of widespread tabular ephemeral fluvial deposits and damp and wet interdunes, which are comparable to those examples of fluvial incursions into aeolian dune fields associated

683 with variable groundwater levels. The resulting dry-wet cycles in the aeolian–fluvial
684 interaction system are a direct indocator of basin-scale climate variability, which
685 dominates the development, expansion and contraction of erg-margin depositional
686 systems. In addition, the rate of tectonic subsidence dictates the preservation of the
687 overall sedimentary stratal architecture (Howell and Mountney, 1997; Mountney et al.,
688 1999; Cosgrove et al., 2022). The presence of wet interdunes and relatively thick
689 sedimentary cycles in the third type of fluvial–aeolian interaction possibly indicates a
690 relatively rapid subsidence rate, which facilitates the accumulation and preservation of
691 sedimentary successions into stratigraphic record. This is similar to other exmaples,
692 such as the Piauí Formation (Kifumbi et al., 2022).

693 The Chaling fluvial–aeolian depositional system is characterized by alternating
694 ephemeral fluvial channels and aeolian deposits. They display similarities to the
695 Permian Cutler Group of the Paradox Basin (Langford and Chan, 1989; Mountney and
696 Jagger, 2004; Jordan and Mountney, 2010; Cain and Mountney, 2011), the Lower
697 Jurassic Kayenta and Navajo Sandstone formations on the Colorado Plateau (Herries,
698 1993; Hassan et al., 2018), and the Lower Cretaceous Twyfelfontein Formation of the
699 Huab Basin (Mountney et al., 1998, 1999), in which periodic flooding led to erosion of
700 aeolian deposits and variable groundwater levels. Damp and wet interdune deposits and
701 drying- or wetting-upwards cycles bounded by flood surfaces and sand-drift surfaces
702 developed in these units. The variations in depositional styles reflect climatic and
703 tectonic controlling mechanisms. The main difference among these basins is that the
704 Permian Cutler Group and the Lower Jurassic Kayenta and Navajo Sandstone

formations developed in a foreland basin setting, whereas the Upper Cretaceous Daijiaping Formation accumulated in a rift environment. All record basin-scale tectono-stratigraphic architectural relationship.

6.4. Implications for East Asian paleoclimate and paleogeography

The Cretaceous in South China Block is characterized by large-scale taphrogeny and magmatism, generating significant extensional basins and igneous provinces (Li et al., 2014b, 2019, 2020). Some models propse a notable distinct compression event during the early Late Cretaceous (100–89 Ma) (Charvet et al., 2013; Yang, 2013; Song et al., 2015) and the formation of the Cathaysian coastal mountains along the South China margin by crustal thickening (Chen, 2000; Yang, 2013; Zhang et al., 2016; Li et al., 2018; Suo et al., 2019; Chen et al., 2021). This compressional event is also evidenced by the occurrence of significant westward provenance in the Danxia, Hengyang and Yuanma hinterland basins (Yan et al., 2011; Yang et al., 2020), which is also recorded in the Chaling alluvial deposits (Fig. 2). Simutaneously, some salars (saline lakes) and aeolian deserts developed in the intermontane basins at the South China margin (Fig. 19). The tectonic and paleoenvironmental characteristics indicate an Andean-type continental margin (Suo et al., 2019). The altitudes of the salars of Atacama, Uyuni and Hombre Muerto in the Andean Plateau of South America are 2300 m, 3663 m and 3970 m, respectively (López-Steinmetz et al., 2018). Salars in the coastal mountain ranges along the East Asian continental margin could have developed at a comparable paleoelevation.

The extensive aeolian desert depositional systems in South China were constructed

and preserved during the Late Cretaceous; the uplifts along the East Asian margin caused the rain-shadow effect and led to the desertification in the South China hinterland combined with sub-tropical highs in the middle and low latitudes of the Northern Hemisphere (Fig. 19), as supported by the divergent paleowind pattern recorded in the aeolian cross-bedded sandstones (Fig. 2). Furthermore, monsoonal water or meltwater discharge carried extra-formational clasts into receiving desert basins and led to variations in the groundwater level, characteristic of dry and wet aeolian dune-field margin systems (Fig. 16). Periodic water influx to the Late Cretaceous Chaling desert margins created a cyclic aeolian–fluvial interaction system (Figs. 17, 18). Overall, the formation and development of Late Cretaceous aeolian desert systems in East Asia reflects the entaglement of subtropical highs, epi- and intra-continental orogeny, and variable groundwater level controlled by a monsoon climate and ongoing tectonic basin subsidence.

7. Conclusions

The Upper Cretaceous Daijiaping Formation exposed in the Chaling Basin of southeast China can be subdivided into two distinct sedimentary units on the basis of sedimentological and facies architectural analyses. The base of this formation consists of (i) pebble-cobble conglomerate and sandstone of streamflow origin accumulated in fluvial channels, and (ii) sand to clay sheetflow deposits and floodplain deposits, all associated with a wadi system that drained from the highland to the east. This succession is overlain by a unit of mixed aeolian and fluvial origin that records simple and compound crescentic aeolian dunes and aeolian sandsheets, deposits of which occur

749 interbedded with restricted channelized bedload stream and cobble-sand sheetflow
750 deposits. In addition, deflation lags, desert pavements, aeolian pods, and damp and wet
751 interdunes developed in this unit.

752 The alternating activity of wind and water resulted in the vertically repeating
753 occurrences of these facies associations. Aeolian deflation of the water-lain sediments
754 is recorded by the presence of deflation lags and desert pavements. Sudden water
755 influxes eroded and reworked aeolian dunes and sandsheets and produced aeolian pods.
756 The presence of damp and wet interdunes records fluctuations of the phreatic water-
757 table level. Two hypotheses are proposed to explain the presence of sudden water
758 influxes into the Chaling erg-margin system: monsoonal water discharge and meltwater
759 fluxes from the eastern highland to the desert margin system. Through the entire
760 aeolian–fluvial unit, numerous wetting-upward cycles are identified. The abrupt nature
761 of transitions between different facies associations and the presence of erosive surfaces
762 (flood surfaces and sand-drift surfaces) together indicate climate-controlled variations
763 in the relative water-table position, sand availability, sediment supply, aeolian and
764 fluvial transport capacity. Cycle preservation indicates the long-term relative rise of the
765 groundwater level as a consequence of long-term fault-driven basin subsidence.

766 Aeolian and fluvial deposition in this erg-margin sedimentary system was
767 dominantly controlled by the climate. Tectonic subsidence enabled the long-term
768 preservation of the accumulated succession. The presence of extensively developed
769 aeolian desert depositional systems in East Asia during the Late Cretaceous is the result
770 of the regional climate; their long-term preservation is enabled by tectonic basin

771 subsidence associated with paleo-Pacific Plate subduction and rollback.

772 **Acknowledgements**

773 We would like to thank Peng Chen and Donghong Li for their help during the field
774 work. The study was supported by the National Key Research and Development
775 Program of China (2023YFC2906605) and the Scientific Research Fund of the China
776 Central Non-Commercial Institute (KK2005 and KK2322).

777 **References**

778 Al-Farraj, A., Harvey, A.M., 2000. Desert pavement characteristics on wadi terrace and
779 alluvial fan surfaces: Wadi Al-Bih, U.A.E. and Oman. Geomorphology 35, 279–
780 297.

781 Al-Farraj, A., Harvey, A.M., 2004. Late Quaternary interactions between aeolian and
782 fluvial processes: a case study in the northern UAE. Journal of Arid Environments
783 56, 235–248.

784 Al-Masrahy, M.A., Mountney, N.P., 2015. A classification scheme for fluvial–aelolian
785 system interaction on desert-margin settings. Aeolian Research 17, 67–88.

786 Amarante, F.B., Scherer, C.M.S., Aguilar, C.A.G., Reis, A.D., Mesa, V., Soto, M., 2019.
787 Fluvial-eolian deposits of the Tacuarembo formation (Norte Basin-Uruguay):
788 Depositional models and stratigraphic succession. Journal of South American
789 Earth Sciences 90, 355–376.

790 Basilici, G., Colombera, L., Soares, M.V.T., Arévalo, O.J., Mountney, N.P., Lorenzoni,
791 P., Filho, C.R.S., Mesquita, Á.F., Janočko, J., 2022. Variations from dry to aquic
792 conditions in Vertisols (Esplugafreda Formation, Eastern Pyrenees, Spain):

793 Implications for late Paleocene climate change. Palaeogeography,
794 Palaeoclimatology, Palaeoecology 595, 110972.
795 Basilici, G., Lorenzoni, P., Mesquita, Á.F., Janočko, J., Colombera, L., Cosgrove, G.I.E.,
796 Mountney, N.P., Filho, C.R.S., Cardoso, A.R., Martinelli, A.G., Fiorelli, L.E.,
797 Garcia, R.G.V., Marinho, T.S., Marconato, A., 2024. Can palaeosols reveal
798 palaeoenvironmental variability of fluvial systems? An example from the upper
799 portion of the Bauru Group (Upper Cretaceous, SE Brazil). Sedimentary Geology
800 464, 106604.
801 Bertolini, G., Hartley, A.J., Marques, J.C., Healy, D., Frantz, J.C., 2021. The effects of
802 basaltic lava flows on the petrophysical properties and diagenesis of interbedded
803 aeolian sandstones: an example from the Cretaceous Paraná Basin, Brazil.
804 Petroleum Geoscience 27, pp. petgeo2020-036.
805 BGMRH, Bureau of Geology, Mineral Resources of Hunan Province. 1984. Regional
806 Geology of Hunan Province. Geological Publishing House, Beijing pp. 208–223
807 (in Chinese with English abstract).
808 Blair, T.C., 1999. Sedimentology of gravelly Lake Lahontan high-stand shoreline
809 deposits, Churchill Butte, Nevada. Sedimentary Geology 123, 187–206.
810 Bridge, J.S., 2003. Rivers and floodplains, forms, processes, and sedimentary record.
811 Blackwell Publishing, Oxford, UK.
812 Brookfield, M.E., 1977. The origin of bounding surfaces in ancient aeolian sandstones.
813 Sedimentology 24, 303–332.
814 Burns, C.E., Mountney, N.P., Hodgson, D.M., Colombera, L., 2019. Stratigraphic

architecture and hierarchy of fluvial overbank splay deposits. Journal of the Geological Society 176, 629–649.

Cain, S.A., Mountney, N.P., 2011. Downstream changes and associated fluvial–eolian interactions in an ancient terminal fluvial system: The Permian Organ Rock Formation, SE Utah, U.S.A. SEPM Special Publication 97, 167–185.

Chakraborty, T., Chaudhuti, A.K., 1993. Fluvial–aeolian interactions in a Proterozoic alluvial plain: Example from the Mancheral Quartzite, Sullavai Group, Pranhita-Gadavari Valley, India. Geological Society Special Publication 72, 127–141.

Charvet, J., 2013. Late Paleozoic-Mesozoic tectonic evolution of SW Japan: a review – reappraisal of the accretionary orogeny and revalidation of the collisional model. Journal of Asian Earth Sciences 72, 88–101.

Charvet, J., Shu, L.S., Shi, Y.S., Guo, L.Z., Faure, M., 1996. The building of South China: collision of Yangzi and Cathaysia blocks, problems and tentative answers. Journal of Southeast Asian Earth Sciences 13, 223–235.

Chen, J.F., Foland, K.A., Xing, F.M., Xu, X., Zhou, T.X., 1991. Magmatism along the southeast margin of the Yangtze block: Precambrian collision of the Yangtze and Cathysia blocks of China. Geology 19, 815–818.

Chen, J.M., Zhao, P., Wang, C.S., Huang, Y.J., 2009. Modelling the East Asian climate during the late cretaceous (80 Ma). Earth Science Frontier 16, 226–239.

Chen, P.J., 2000. Paleoenvironmental changes during the Cretaceous in eastern China. In Hakuyu, O., and Nlall, J.M., eds, Developments in Palaeontology and Stratigraphy. Elsevier pp. 81–90.

837 Chen, Y., Meng, J., Liu, H., Wang, C.S., Tang, M., Liu, T., Zhao, Y.N., 2021. Detrital
838 zircons record the evolution of the Cathaysian Coastal Mountains along the South
839 China margin. Basin Research 34, 688–701.
840 Chu, C., 1978. Red rock series in Youxian and Chaling, Hunan. Acta Stratigraphica
841 Sinica 2, 146–151 (in Chinese).
842 Clemmensen, L.B., 1989. Preservation of interdraa and plinth deposits by the lateral
843 migration of large linear draas (Lower Permian Yellow Sands, northeast England).
844 Sedimentary Geology 65, 139–151.
845 Clemmensen, L.B., Tirsgaard, H., 1990. Sand-drift surfaces: a neglected type of
846 bounding surface. Geology 18, 1142–1145.
847 Clemmensen, L.C., Abrahamsen, K., 1983. Aeolian stratification and facies association
848 in desert sediments, Arran basin (Permian), Scotland. Sedimentology 30, 311–339.
849 Colombera, L., Mountney, N.P., 2021. Influence of fluvial crevasse-splay deposits on
850 sandbody connectivity: Lessons from geological analogues and stochastic
851 modelling. Marine and Petroleum Geology, 128, 105060.
852 Cosgrove, G.I.E., Colombera, L., Mountney, N.P., 2022. The role of subsidence and
853 accommodation generation in controlling the nature of the aeolian stratigraphic
854 record. Journal of the Geological Society 179, jgs2021-042.
855 Cowan, G., 1993. Identification and significance of aeolian deposits within the
856 dominantly fluvial Sherwood Sandstone Group of the East Irish Sea Basin UK.
857 Geological Society, London, Special Publication 73, 231–245.
858 Dávila, F.M., Astini, R.A., 2003. Las eolianitas de la Sierra de Famatina (Argentina):

859 interacción paleoclima-tectónica en el antepaís fragmentado andino central
860 durante el Mioceno Medio. Revista geológica de Chile 30, 187–204.
861 Dias, K.D.N., Scherer, C.M.S., 2008. Cross-bedding set thickness and stratigraphic
862 architecture of aeolian systems: an example from the Upper Permian Pirambóia
863 Formation (Paraná Basin), southern Brazil. Journal of South American Earth
864 Sciences 25, 405–415.
865 Dorn, R.I., 1990. Quaternary alkalinity fluctuations recorded in rock varnish
866 microlaminations on western U.S.A. volcanics. Palaeogeography,
867 Palaeoclimatology, Palaeoecology 76, 291–310.
868 Duan, J.R., Peng, E.S., Wei, Z.L., 1978. Lithofacies of Cretaceous-Tertiary red beds in
869 Chayong Basin, Hunan province. Geotectonica et Metallogenia 2, 13–41 (in
870 Chinese).
871 Ellis, D., 1993. The Rough Gas Field: distribution of Permian aeolian and non-aeolian
872 reservoir facies and their impact on field development. Geological Society,
873 London, Special Publication 73, 265–277.
874 Farnsworth, A., Lunt, D.J., Robinson, S.A., Valdes, P.J., Roberts, W.H.G., Clift, P.D.,
875 Markwick, P., Su, T., Wrobel, N., Bragg, F., Kelland, S.J., Pancost, R.D., 2019.
876 Past East Asian mosoon evolution controlled by paleogeography, not CO_2. Science
877 Advances 5, 1–13.
878 Ferronatto, J.P.F., Scherer, C.M.S., Souza, E.G., Reis, A.D., Mello, R.G., 2019. Genetic
879 units and facies architecture of a Lower Cretaceous fluvial-aeolian succession, São
880 Sebastião Formation, Jatobá Basin, Brazil. Journal of South American Earth

881 Sciences 89, 158–172.
882 Frederiksen, K.S., Clemmensen, L.B., Lawaetz, H.S., 1998. Sequential architecture and
883 cyclicity in Permian desert deposits, Brodick Beds, Arran, Scotland. Journal of the
884 Geological Society 155, 677–683.
885 Fryberger, S.G., Al-Sari, A.M., Clisham, T.J., 1983. Eolian dune, interdune, sand sheet,
886 and siliciclastic sabkha sediments of an offshore prograding sand sea, Dhahran
887 area, Saudi Arabia. American Association of Petroleum Geologists Bulletin 67,
888 280–312.
889 Fryberger, S.G., Hesp, P., Hastings, K., 1992. Aeolian granule ripple deposits, Namibia.
890 Sedimentology 39, 319–331.
891 Gao, H.X., 1975. Paleocene mammal-bearing beds of Chaling Basin, Hunan. Vertebrata
892 Palasiatica 13, 89–95 (in Chinese with English abstract).
893 Ghazi, S., Mountney, N.P., 2009. Facies and architectural element analysis of a
894 meandering fluvial succession: The Permian Warchha Sandstone, Salt Range,
895 Pakistan. Sedimentary Geology 221, 99–126.
896 Glennie, K.W., 1970. Desert Sedimentary Environments. Elsevier pp. 222.
897 Gradzinski, R., Jerzykiewicz, T., 1974. Dinosaur-and mammal-bearing aeolian and
898 associated deposits of the Upper Cretaceous in the Gobi Desert (Mongolia).
899 Sedimentary Geology 12, 249–278.
900 Hassan, M.S., Venetikidis, A., Bryant, G., Miall, A.D., 2018. The sedimentology of an
901 erg margin: The Kayenta–Navajo transition (Lower Jurassic), Kanab, Utah, U.S.A.
902 Journal of Sedimentary Research 88, 613–640.

903 Henares, S., Bloemsma, M.R., Donselaar, M.E., Mijnlieff, H.F., Redjosentono, A.E.,
904 Veldkamp, H.G., Weltje, G.J., 2014. The role of detrital anhydrite in diagenesis of
905 aeolian sandstones (Upper Rotliegend, The Netherlands): Implications for
906 reservoir-quality prediction. Sedimentary Geology 314, 60–74.
907 Herries, R.D., 1993. Contrasting styles of fluvial–aeolian interaction at a downwind erg
908 margin: Jurassic Kayenta–Navajo transition, northern Arizona, USA. Geological
909 Society Special Publication 73, 199–218.
910 Herries, R.D., Cowan, G., 1997. Challenging the 'sheetflood'myth: the role of
911 watertable-controlled sabkha deposits in redefining the depositional model for the
912 Ormskirk Sandstone Formation (Lower Triassic), East Irish Sea Basin. Geological
913 Society, London, Special Publication 124, 253–276.
914 Howell, J.A., Mountney, N.P., 1997. Climatic cyclicity and accommodation space in
915 arid to semi-arid depositional systems: an example from the Rotliegend Group of
916 the Southern North Sea. In: Ziegler, K., Turner, P., and Daines, S.R., eds.,
917 Petroleum Geology of the Southern North Sea: Future Potential. Geological
918 Society, London, Special Publication 123, 63–86.
919 Hunter, R.E., 1977. Basic types of stratification in small eolian dunes. Sedimentology
920 24, 361–387.
921 Jiang, X.S., Pan, Z.X., Xu, J.S., Li, X.Y., Xie, G.G., Xiao, Z.J., 2008. Late Cretaceous
922 Aeolian dunes and reconstruction of palaeowind belts of the Xinjiang Basin,
923 Jiangxi Province, China. Palaeogeography, Palaeoclimatology, Palaeoecology 257,
924 58–66.

925 Jiao, H.J., Wu, C.H., Rodríguez-López, J.P., Sun, X.M., Yin, H.S., 2020. Late
926 Cretaceous plateau deserts in the South China Block, and Quaternary analogues;
927 sedimentology, dune reconstruction and wind-water interactions. Marine and
928 Petroleum Geology 120, 104504.
929 Jones, F.H., Scherer, C.M.S., Kuchle, J., 2016. Facies architecture and stratigraphic
930 evolution of aeolian dune and interdune deposits, Permian Caldeirão Member
931 (Santa Brígida Formation), Brazil. Sedimentary Geology 337, 133–150.
932 Jordan, O.D., Mountney, N.P., 2010. Styles of interaction between aeolian, fluvial and
933 shallow marine environments in the Pennsylvanian to Permian lower Cutler beds,
934 south-east Utah, USA. Sedimentology 57, 1357–1385.
935 Kifumbi, C., Scherer, C.M.S., Souza, E.G., Reis, A.D., Ferronatto, J.P.F., Michel,
936 R.D.L., 2022. Late Pennsylvanian aridification in Gondwana mid-latitudes
937 contemporaneous to high-latitudes ice cap expansion, upper Piauí Formation,
938 Brazil. Journal of South American Earth Sciences 117, 103810.
939 Knight, J., 2008. The environmental significance of ventifacts: a critical review. Earth-
940 Science Reviews 86, 89–105.
941 Kocurek, G., 1981. Significance of interdune deposits and bounding surfaces in aeolian
942 dune sands. Sedimentology 28, 753–780.
943 Kocurek, G., 1988. First-order and super bounding surfaces in eolian sequences –
944 bounding surfaces revisited. Sedimentary Geology 56, 193–206.
945 Kocurek, G., 1991. Interpretation of ancient eolian sand dunes. Annual Review of Earth
946 and Planetary Sciences 19, 43–75.

947 Kocurek, G., 1996. Desert aeolian systems. In: Reading, H.G., ed., Sedimentary
948 Environments: Processes, Facies and Stratigraphy. Blackwell Science, Oxford, pp.
949 125–153.
950 Kocurek, G., 1999. The aeolian rock record (Yes, Virginia, it exists, but it really is rather
951 special to create one). In Goudie, A., and Livingtone, I., eds., Aeolian
952 Environments, Sediments and Landforms. John Wiley and Sons, New York, pp.
953 239–259.
954 Kocurek, G., Havholm, K.G., 1993. Eolian sequence stratigraphy – a conceptual
955 framework. In: Weimer, P., and Posamentier, H.W., eds., Siliciclastic Sequence
956 Stratigraphy: Recent Developments and Applications. SEPM Special Publication
957 52, 393–409.
958 Kocurek, G., Lancaster, N., 1999. Aeolian system sediment state: theory and Mojave
959 Desert Kelso dunefield example. Sedimentology 46, 477–504.
960 Kocurek, G., Nielson, J., 1986. Conditions favourable for the formation of warm-
961 climate aeolian sand sheets. Sedimentology 33, 495–816.
962 Lacotte, V.J.P.H., Mountney, N.P., 2022. A classification scheme for sedimentary
963 architectures arising from aeolian-fluvial system interactions: Permian examples
964 from southeast Utah, USA. Aeolian Research 58, 100815.
965 Lancaster, N., Mountney, N.P., 2021, Aeolian Processes and Sediments. In: Alderton,
966 D., and Elias, S., eds., Encyclopedia of Geology (Second Edition): Elsevier, p.
967 809–829.
968 Langford, R., Chan, Y., 1988. Flood surfaces and deflation surfaces within the Cutler

969 Formation and Cedar Mesa Sandstone (Permian), Southern Utah. Geological
970 Society of America Bulletin 100, 1541–1549.
971 Langford, R.P., 1989. Fluvial–aeolian interactions. Part I. Modern systems.
972 Sedimentology 36, 1023–1035.
973 Langford, R.P., Chan, M.A., 1989. Fluvial–aeolian interactions. Part II. Ancient
974 systems. Sedimentology 36, 1037–1051.
975 Li, J.H., Cawood, P.A., Ratschbacher, L., Zhang, Y., Dong, S., Xin, Y., Yang, H., Zhang,
976 P.X., 2020. Building Southeast China in the late Mesozoic: Insights from
977 alternating episodes of shortening and extension along the Lianhuashan fault zone.
978 Earth-Science Reviews 201, 103056.
979 Li, J.H., Dong, S.W., Cawood, A., Zhao, G., Johnston, S.T., Zhang, Y., Xin, Y., 2018.
980 An Andean-type retro-arc foreland system beneath northwest South China
981 revealed by SINOPROBE profiling. Earth and Planetary Science Letters 490, 170–
982 179.
983 Li, J.H., Ma, Z.L., Zhang, Y.Q., Dong, S.W., Li, Y., Lu, M.A., Tan, J.Q., 2014a. Tectonic
984 evolution of Cretaceous extensional basins in Zhejiang Province, eastern South
985 China: structural and geochronological constraints. International Geology
986 Reviews 56, 1602–1629.
987 Li, J.H., Zhang, Y.Q., Dong, S.W., Johnston, S.T., 2014b. Cretaceous tectonic evolution
988 of South China: a preliminary synthesis. Earth-Science Reviews 56, 1602–1629.
989 Li, J.H., Zhang, Y.Q., Dong, S.W., Shi, W., 2013. Structural and geochronological
990 constraints on the Mesozoic tectonic evolution of the North Dabashan zone, South

991 Qinling, central China. Journal of Asian Earth Sciences 64, 99–114.
992 Li, S.Z., Suo, Y.H., Li, X.Y., Zhou, J., Santosh, M., Wang, P.C., Wang, G.Z., Guo, L.L.,
993 Yu, S.Y., Lan, H.Y., Dai, L.M., Zhou, Z.Z., Cao, X.Z., Zhu, J.J., Liu, B., Jiang,
994 S.H., Wang, G., Zhang, G.W., 2019. Mesozoic tectono-magmatic response in the
995 East Asian ocean-continent connection zone to subduction of the Paleo-Pacific
996 Plate. Earth-Science Reviews 192, 91–137.
997 Li, X., Yi., C., Chen, F., Ya, T., Li., X., 2006. Formation of proglacial dunes in front of
998 the Puruogangri Icefield in the central Qinghai–Tibet Plateau: implications for
999 reconstructing paleoenvironmental changes since the Late glacial. Quaternary
1000 International 154–155, 122–127.
1001 Liu, R.C., 2018. Paleoclimate of the Late Cretaceous-Paleocene in the Chaling Basin,
1002 Hunan, South China. Master dissertation, Nanjing University (in Chinese with
1003 English abstract).
1004 Loope, D.B., Rowe, C.M., Joeckel, R.M., 2001. Annual monsoon rains recorded by
1005 Jurassic dunes. Nature 412, 64–66.
1006 López-Steinmetz, R.L., Salvi, S., Garcia, M.G., Arnold, Y.P., Beziat, D., Franco, G.,
1007 Constantini, O., Cordoba, F.E., Caffe, P.J., 2018. Northern Puna plateau-scale
1008 survey of Li brine-type deposits in the Andes of NW Argentina. J. Geochem.
1009 Explor. 190, 26–38.
1010 Mack, G.H., Leeder, M.R., Carothers-Durr, M., 2008. Modern flood deposition, erosion,
1011 and fan-channel avulsion on the semiarid Red Canyon and Palomas Canyon
1012 alluvial fans in the southern Rio Grande Rift, New Mexico, USA. J. Sed. Res. 78,

1013 432–442.
1014 Malmon, D.V., Reneau, S.L., Dunne, T., 2004. Sediment sorting and transport by flash
1015 floods. Journal of Geophysical Research: Earth Surface 109, F02005.
1016 Mayoral, J.P., Scotti, A.A., Apesteguía, S., Veiga, G., 2021. High-resolution analysis of
1017 an erg-margin system from the cretaceous Candeleros Formation (La Buitrera
1018 paleontological area, Río Negro province, Argentina): An approach to different
1019 scales of fluvial-aeolian interactions. Latin American Journal of Sedimentology
1020 and Basin Analysis 28, 37–59.
1021 Miall, A., 1996. Geology of fluvial deposits. Berlin, SpringerVerlag, pp. 582.
1022 Mountney, N., Howell, J., Flint, S., Jerram, D., 1998. Aeolian and alluvial deposition
1023 within the Mesozoic Etjo Sandstone Formation, northwest Namibia. Journal of
1024 African Earth Sciences 27, 175–192.
1025 Mountney, N., Howell, J., Flint, S., Jerram, D., 1999. Climate, sediment supply and
1026 tectonics as control on the deposition and preservation of aeolian–fluvial Etjo
1027 Sandstone Formation, Namibia. J. Geol. Soc. London 156, 771–777.
1028 Mountney, N.P., 2004. Feature: the sedimentary signature of deserts and their response
1029 to environmental change: Geology Today 20, 101–106.
1030 Mountney, N.P., 2006. Periodic accumulation and destruction of aeolian erg sequences
1031 in the Permian Cedar Mesa Sandstone, White Canyon, southern Utah, USA.
1032 Sedimentology 53, 789–823.
1033 Mountney, N.P., 2012. A stratigraphic model to account for complexity in aeolian dune
1034 and interdune successions. Sedimentology 59, 964–989.

Mountney, N.P., Jagger, A., 2004. Stratigraphic evolution of an aeolian erg margin system: the Permian Cedar Mesa Sandstone, SE Utah, USA. Sedimentology 51, 1–31.

Mountney, N.P., Thompson, D.B., 2002. Stratigraphic evolution and preservation of aeolian dune and damp/wet interdune strata: an example from the Triassic Helsby Sandstone Formation, Cheshire Basin, UK. Sedimentology 49, 805–833.

Nemec, W., Postma, G., 1993. Quaternary alluvial fans in southwestern Crete: sedimentation processes and geomorphic evolution. In: Marzo, M., and Puigdefabregas, C., eds., Alluvial Sedimentation. IAS Special Publication, 17, 235–276.

Newell, A.J., 2001. Bounding surfaces in a mixed aeolian–fluvial system (Rotliegend, Wessex Basin, SW UK). Marine and Petroleum Geology 18, 339–347.

Porter, M.L., 1987. Sedimentology of an ancient erg margin: the Lower Jurassic Aztec Sandstone, southern Nevada and southern California. Sedimentology 34, 661–680.

Priddy, C.L, Clarke, S.M., 2020. The sedimentology of an ephemeral fluvial–aeolian succession. Sedimentology 67, 2392–2425.

Reis, A.D.D., Scherer, C.M.S., Amarante, F.B.D., Rossetti, M.D.M.M., Kifumbi, C., Souza, E.G.D., Ferronatto, J.P.F., Owen, A., 2019. Sedimentology of the proximal portion of a large-scale, Upper Jurassic fluvial-aeolian system in Paraná Basin, southwestern Gondwana. Journal of South American Earth Sciences 95, 102248.

Reis, A.D.D., Scherer, C.M.S., Owen, A., Amarante, F.B.D., Ferronatto, J.P.F., Pantopoulos, G., Souza, E.G.D., Bállico, M.B., Aguilar, C.A.G., 2022. A

quantitative depositional model of a large distributive fluvial system (Megafan) with terminal aeolian interaction: The Upper Jurassic Guará DFS in southwestern Gondwana. Journal of Sedimentary Research 92, 460–485.

Retallack, G.J., 1994. The environmental factor approach to the interpretation of paleosols. SSSA Special Publication 33, 31–64.

Rodríguez-López, J.P., Liesa, C.L., Van Dam, J., La Fuente, P., Arlegui, L., Ezquerro, L., DeBore, P., 2012. Aeolian construction and alluvial dismantling of a fault-bounded intracontinental aeolian dune field (Teruel Basin, Spain); a continental perspective on Late Pliocene climate change and variability. Sedimentology 59, 1536–1567.

Rodríguez-López, J.P., Meléndez, N., de Boer, P.L., Soria, A.R., 2010. The action of wind and water in a back erg margin system close to the Variscan Iberian Massif. Sedimentology 57, 1315–1356.

Rodríguez-López, J.P., Meléndez, N., de Boer, P.L., Soria, A.R., Liesa, C.L., 2013. Spatial variability of multi-controlled aeolian supersurfaces in central-erg and marine–erg–margin systems. Aeolian Research 11, 141–154.

Rodríguez-López, J.P., Wu, C.H., 2020. Recurrent deformations of aeolian desert dunes in the Cretaceous of the South China Block: trigger mechanisms variability and implications for aeolian reservoirs. Marine and Petroleum Geology 119, 104483.

Rubin, D.M., 1987. Cross-bedding, bedforms and palaeocurrents. SEPM Concepts in Sedimentology and Paleontology 1, pp. 187.

Scherer, C.M.S., 2000. Eolian dunes of the Botucatu Formation (Cretaceous) in

1079 southernmost Brazil: morphology and origin. Sedimentary Geology 137, 63–84.
1080 Scherer, C.M.S., Lavina, E.L.C., 2005. Sedimentary cycles and facies architecture of
1081 aeolian–fluvial strata of the Upper Jurassic Guará Formation, southern Brazil.
1082 Sedimentology 52, 1323–1341.
1083 Scherer, C.M.S., Lavina, E.L.C., 2006. Stratigraphic evolution of a fluvial–eolian
1084 succession: The example of the Upper Jurassic–Lower Cretaceous Guará and
1085 Botucatu formations, Paraná Basin, southernmost Brazil. Gondwana Research 9,
1086 475–484.
1087 Scherer, C.M.S., Lavina, E.L.C., Dias Filho, D.C., Oliveira, F.M., Bongiolo, D.E.,
1088 Aguiar, E.S., 2007. Stratigraphy and facies architecture of the fluvial–aeolian–
1089 lacustrine Sergi Formation (Upper Jurassic) Recmŏcavo Basin, Brazil.
1090 Sedimentary Geology 194, 169–193.
1091 Shu, L.S., Faure, M., Wang, B., Zhou, X.M., Song, B., 2008. Late Palaeozoic–Early
1092 Mesozoic geological features of South China: response to the Indosinian collision
1093 events in Southeast Asia. Comptes Rendus Geoscience 340, 151–165.
1094 Shu, L.S., Zhou, X.M., Deng, P., Wang, B., Jiang, S.Y., Yu, J.H., Zhao, X.X., 2009.
1095 Mesozoic tectonic evolution of the Southeast China Block: new insights from
1096 basin analysis. Journal of Asian Earth Sciences 34, 376–391.
1097 Simpson, E.L., Hilbert-Wolf, H.L., Simpson, W.S., Tindall, S.E., Bernard, J.J., Jenesky,
1098 T.A., Wizevich, M.C., 2008. The interaction of aeolian and fluvial processes
1099 during deposition of the Upper Cretaceous capping sandstone member, Wahweap
1100 Formation, Kaiparowits Basin, Utah, U.SA. Palaeogeography, Palaeoclimatology,

Palaeoecology 270, 19–28.

Smith, D.G., Cross, T.A., Dufficy, J.P., Clough, S.R., 1989. Anatomy of an avulsion. Sedimentology 36, 1–23.

Smith, R.A., Jones, N.S., Monaghan, A.A., Arkley, S., 2006. Fluvial and aeolian deposition in the Siluro-Devonian Swanshaw Sandstone Formation, SW Scotland. Scottish Journal of Geology 42, 161–177.

Soares, M.V.T., Basilici, G., Lorenzoni, P., Colombera, L., Mountney, N.P., Martinelli, A.G., Mesquita, A.F., Marinho, T.S., Vasconez, R.G.G., Marconato, A., 2020. Landscape and depositional controls on palaeosols of a distributive fluvial system (Upper Cretaceous, Brazil). Sedimentary Geology 409, 105774.

Song, Y., Stepashko, A.A., Ren, J., 2015. The Cretaceous climax of compression in Eastern Asia: Age 87–89 Ma (late Turonian/Coniacian), Pacific cause, continental consequences. Cretac. Res. 55, 262–284.

Spalletti, L.A. and Veiga, G.D., 2007. Variability of continental depositional systems during lowstand sedimentation: An example from the Kimmeridgian of the Neuquen Basin, Argentina. Latin American Journal of Sedimentology and Basin Analysis 14, 85–104.

Spalletti, L.A., Limarino, C.O., Pinol, F.C., 2010. Internal anatomy of an erg sequence from the aeolian–fluvial system of the Da La Cuesta Formation (Paganzo Basin, northwestern Argentina). Geological Acta 8, 431–447.

Stanistreet, I.G., Stollhofen, H., 2002. Hoanib River flood deposits of Namib Desert interdunes as analogues for thin permeability barrier mudstone layers in aeolianite

reservoirs. Sedimentology 49, 719–736.

Sun, Z., Yang, Z., Yang, T., Pei, J., Yu, Q., 2006. New Late Cretaceous and Paleogene paleomagnetic results from south China and their geodynamic implications. Journal of Geophysical Research: Solid Earth 111, 1581–1600.

Suo, Y., Li, S., Jin, C., Zhang, Y., Zhou, J., Li, X., Wang, P., Liu, Z., Wang, X., Somerville, I., 2019. Eastward tectonic migration and transition of the Jurassic-Cretaceous Andean-type continental margin along Southeast China. Earth-Science Reviews 196, 102884.

Svendsen, J., Stollhofen, H., Krapf, C.B.E., Stanistreet, I.G., 2003. Mass and hyperconcentrated flow deposits record dune damming and catastrophic breakthrough of ephemeral rivers, Skelton Coast Erg, Namibia. Sed. Geol. 160, 7–31.

Sweet, M.P., 1999. Interaction between aeolian, fluvial and playa environments in the Permian Upper Rotliegend Group, UK southern North Sea. Sedimentology 46, 171–187.

Tan, J., Zhang, L.M., Wang, C.S., Cao, K., Li, X., 2020. Late Cretaceous provenance change in the Jiaolai Basin, East China: Implications for paleogeographic evolution of East Asia. Journal of Asian Earth Sciences, 194, 104188.

Tanner, L.H., Hubert, J.F., 1992. Depositional facies, palaeogeography and palaeoclimatology of the Lower Jurassic McCoy Brook Formation, Fundy rift basin, Nova Scotia. Palaeogeogr. Palaeoclimatol. Palaeoecol. 96, 261–280.

Tirsgaard, H., Øxnevad, I.E.I., 1998. Preservation of pre-vegetational mixed fluvio–

1145 aeolian deposits in a humid climatic settings: An example from the Middle
1146 Proterozoic Eriksfjord Formation, Southwest Greenland. Sedimentary Geology
1147 120, 295–317.
1148 Todd, S.P., 1989. Stream-driven, high-density gravelly traction carpets: possible
1149 deposits in the Trabeg Conglomerate Formation, SW Ireland and some theoretical
1150 considerations of their origin. Sedimentology 36, 513–530.
1151 Trewin, N.H., 1993. Mixed aeolian sandsheet and fluvial deposits in the Tumblagooda
1152 Sandstone, western Australia. Geological Society Special Publication 73, 219–230.
1153 Turner, B.R., Makhlouf, I., 2002. Recent colluvial sedimentation in Jordan: fans
1154 evolving into sand ramps. Sedimentology 49, 1283–1298.
1155 Turner, B.R., Makhlouf, I., 2005. Quaternary sandstones, northeast Jordan: age
1156 depositional environments and climate implications. Palaeogeogr. Palaeoclimatol.
1157 Palaeoecol. 229, 230–250.
1158 Turner, P., 1980. Continental red beds. Dev. Sedimentol. 29, 69–125.
1159 Veiga, G.D., Spalletti, L.A., 2007. The Upper Jurassic (Kimmeridgian) fluvial–aeolian
1160 systems of the southern Neuquén Basin, Argentina. Gondwana Research 11, 286–
1161 302.
1162 Veiga, G.D., Spalletti, L.A., Flint, S., 2002. Aeolian/fluvial interactions and high-
1163 resolution sequence stratigraphy of a non-marine lowstand wedge: the Avilé
1164 Member of the Agrio Formation (Lower Cretaceous), central Neuquén Basin,
1165 Argentina. Sedimentology 49, 1001–1019.
1166 Vieira, L.V., Scherer, C.M.S., 2017. Facies architecture and high resolution sequence

1167 stratigraphy of an aeolian, fluvial and shallow marine system in the Pennsylvanian
1168 Piauí Formation, Parnaíba Basin, Brazil. Journal of South American Earth
1169 Sciences 76, 238–256.
1170 Wakelin-King, G.A., Webb, J.A., 2007. Upper-flow-regime mud floodplains, lower-
1171 flow-regime sand channels: sediment transport and deposition in a drylands mud-
1172 aggregate river. Journal of Sedimentary Research 77, 702–712.
1173 Wang, C.L., 1998. Formation of Luoxiao mountains and development of its Danxia
1174 land feature. Journal of Xiangtan Normal College 19, 110–115 (in Chinese with
1175 English abstract).
1176 Wang, Y.J., Fan, W.M., Cawood, P.A., Ji, S.C., Peng, T.P., Chen, X.Y., 2007.
1177 Indosinian high-strain deformation for the Yunkaidashan tectonic belt, south
1178 China: kinematics and $^{40}Ar/^{39}Ar$ geochronological constraints. Tectonics 26,
1179 TC6008.
1180 Worden, R.H., Burley, S.D., 2003. Sandstone diagenesis: the evolution of sand to stone.
1181 In: Burley, S.D., and Worden, R.H., eds., Sandstone Diagenesis: Recent and
1182 Ancient. Blackwell Publishing pp. 3–44.
1183 Wu, C.H., Rodríguez-López, J.P., Santosh, M., 2022. Plateau archives of lithosphere
1184 dynamics, cryosphere and paleoclimate: The formation of Cretaceous desert
1185 basins in East Asia. Geoscience Frontiers, 13, 101454.
1186 Xi, D.P., Wan, X.Q., Li, G.B., Li, G., 2019. Cretaceous integrative stratigraphy and
1187 timescale of China. Science China Earth Sciences 62, 256–286.
1188 Xiao, B.F., Xiao, H.P., Qi, Y.P., Jing, S.Q., Li, F., 2019. Tectono-geomorphic features

and evolution in less and weak earthquake region based on DEM–a case study in Chaling–Yongxing Basin of Hunan Province. South China Journal of Seimology 39, 147–155 (in Chinese with English abstract).

Xu, H., Liu, Y.Q., Kuang, H.W., Peng, N., 2019. Late Jurassic fluvial–eolian deposits from the Tianchihe Formation, Ningwu–Jingle Basin, Shanxi Province, China. Journal of Asian Earth Sciences 174, 245–262.

Yan, Y., Hu, X.Q., Lin, G., Santosh, M., Chan, L.S., 2011. Sedimentary provenance of the Hengyang and Mayang basins, SE China, and implications for the Mesozoic topographic change in South China Craton: Evidence from detrital zircon geochronology. J. Asian Earth Sci. 41, 494–503.

Yang, Q.J., Liu, F.J., Hua, S., Chen, L., Chen, G.J., Chen, L.Q., 2020. Paleoclimate characteristics and provenance analysis of detrital zircons of aeolian sandstone on Jinshiyan section in Danxia Formation, Danxia Basin, Guangdong Province. Journal of Arid Land Resources and Environment 34, 73–80 (in Chinese with English abstract).

Yang, X., Preusser, F., Radtke, U., 2006. Later Quaternary environmental changes in the Taklamakan Desert, western China, inferred from OSL-dated lacustrine and aeolian deposits. Quatern. Sci. Rev. 25, 923–932.

Yang, Y.T., 2013. An unrecognized major collision of the Okhotomorsk block with East Asia during the late cretaceous, constraints on the plate reorganization of the northwest pacific. Earth-Sci. Rev. 126, 96–115.

Yu, X.C., Liu, C.L., Wang, C.L., Li, F., Wang, J.Y., 2020. Eolian deposits of the north

margin of the South China (Jianghan Basin): reconstruction of the Late Cretaceous East Asian landscape in Central China. Marine and Petroleum Geology 117, 104390.

Yu, X.C., Liu, C.L., Wang, C.L., Wang, J.Y., 2021b. Late Cretaceous aeolian desert system within the Mesozoic fold belt of South China: palaeoclimatic changes and tectonic forcing of East Asian erg development and preservation. Palaeogeography, Palaeoclimatology, Palaeoecology 567, 110299.

Yu, X.C., Wang, C.L., Bertolini, G., Liu, C.L., Wang, J.Y., 2021a. Damp- to dry aeolian systems: Sedimentology, climate forcing, and aeolian accumulation in the Late Cretaceous Liyou Basin, South China. Sedimentary Geology 426, 106030.

Zhang, J., Liu, Y., Flögel, S., Zhang, T., Wang, C., Fang, X., 2021. Altitude of the East Asian coastal mountains and their influence on Asian climate during early Late Cretaceous. Journal of Geophysical Research: Atmospheres 126, e2020JD034413. https://doi. org/10.1029/2020JD034413.

Zhang, L., Wang, C., Cao, K., Wang, Q., Tan, J., Gao, Y., 2016. High elevation of Jiaolai basin during the late cretaceous: implication for the coastal mountains along the East Asian margin. Earth Planet. Sci. Lett. 456, 112–123.

Zhao, B.Q., 1985. Subdivision and correlation of the Upper Cretaceous of Hunan. Hunan Geology 4, 28–35 (in Chinese with English abstract).

Zhao, G.C., Cawood, P.A., 1999. Tectonothermal evolution of the Mayuan assemblage in the Cathaysia Block: new evidence for Neoproterozoic collisional-related assembly of the South China craton. Am. J. Sci. 299, 309–339.

Zhao, J.H., Zhou, M.F., Yan, D.P., Zheng, J.P., Li, J.W., 2011. Reappraisal of the ages of Neoproterozoic strata in South China: no connection with the Grenvillian orogeny. Geology 39, 299–302.

Zhao, Z.H., Bao, Z.W., Zhang, B.Y., 1998. Geochemistry of the Mesozoic basaltic rocks in southern Hunan Province. Science in China Series D-Earth Sciences 41, 102–112.

Zhou, X.M., Sun, T., Shen, W.Z., Shu, L.S., Niu, Y.L., 2006. Petrogenesis of Mesozoic granitoids and volcanic rocks in South China: a response to tectonic evolution. Episodes 29, 26–33.

Figure captions

Fig. 1. (A) Sketch map of tectonic units in China showing the location of the South China Block (Li et al., 2014a). (B) Simplified geological map of South China depicting the distribution of Cretaceous Chaling basin (Li et al., 2014a). (C) Geological map of Chaling Basin. The locations of the studied outcrop sections are indicated.

Fig. 2. Simplified sedimentary logs of the outcrop sections of the Daijiaping Formation

showing the pattern of the paleocurrents. The locations of these sections are shown in Fig. 1C. Section a is modified from Liu (2018). See Table 2 for lithofacies codes.

Fig. 3. (A) and (B) Massive matrix to clast-supported cobble to pebble conglomerates (Gmd) bounded by concave-up erosive surfaces. (C) Trough cross-bedded conglomerates (Gct) with distinct pebble- to cobble-clast imbrications. (D) Clast-supported, trough cross-bedded cobble to pebble conglomerates overlain by pebbly sandstones (Spm). (E) Alternating matrix-supported fine pebble to granule conglomerates (Gmp) and pebbly sandstones (Spm) forming a fining-upward cycle. (F) Matrix-supported fine pebble to granule conglomerates (Gmp) interbedded with planar cross-bedded sandstones (Spx). Scale: The diameter of the camera lens cap is 7.7 cm; the hammer is 38 cm long; the field notebook is 18.2 long and 12.5 wide; the geologist is 1.7 cm tall.

Fig. 4. (A) and (B) Clast-supported, horizontal to low-angle cross-bedded cobble to pebble conglomerates (Gch) with embedded lenticular sandstones. The geologist is 1.7 cm tall. (C) and (D) Planar cross-bedded conglomerates (Gch) containing lens-shaped sandstones. The geologist is 1.8 cm tall. (E) Close-up of (C). (F) Planar cross-bedded conglomerates (Gch) are interbedded with pebbly sandstones (Spm). The field notebook is 18.2 long and 12.5 wide.

Fig. 5. (A) Thick silty mudstones (Fl) overlain matrix-supported conglomerates (Gmi), ripple cross-bedded sandstones (Sr), tabular sandstones (Sm) and lenticular or laminated silty mudstones (Fl) in ascending order. Interbedded tabular sandstones (Sm) and laminated silty mudstones (Fl) develop at the top of the outcrop section. Geologist

for scale is 1.7 m tall. (B) and (C) Close-up of (A). Purple mudstone intraclasts occur in the conglomerates. (D) Alternating tabular sandstones (Sm) and laminated silty mudstones (Fl). (E) Close-up of thick silty mudstones showing pale grey-green mottling, slickensides and siltstone aggregates. The diameter of the camera lens cap is 7.7 cm.

Fig. 6. (A) Laterally continuous quartzite pebbles (Gc(e)) overlain by large-scale tabular cross-bedded sandstones (St(e)). (B) Close-up of quartzite pebbles. These pebbles show polished surfaces and pyramid shapes. (C) Tabular clast-supported conglomerates (Gc(e)) are interbedded with low-angle cross-bedded sandstones (Sl(e)). (D) Tabular clast-supported conglomerates (Gc(e)) with flat base and top surfaces overlain by low-angle cross-bedded sandstones (Sl(e)). Scale: the hammer is 38 cm long; the diameter of the camera lens cap is 7.7 cm.

Fig. 7. (A) Low-angle cross-bedded sandstones (Sl(e)) overlain by large-scale trough cross-bedded sandstones (St(e)). (B) and (C) Laterally continuous limestones and quartzite pebbles (Gc(e)) overlain by low-angle cross-bedded sandstones (Sl(e)). (D) Isolated occurrence of sub-horizontal laminated sandstones (Sl(e)). (E) Close-up of (D) showing the alternation of lags of granules (gr) and wind-ripple deposits (wr). Geologist for scale is 1.7 m tall.

Fig. 8. (A) Field photograph and (B) line drawing of low-angle cross-bedded sandstones (Sl(e)) interbedded with horizontal to low-angle cross-bedded conglomerates (Gch). Discrete pebbles (Gc(e)) pinch out laterally in the low-angle cross-bedded sandstones (Sl(e)).

Fig. 9. (A) Inverse grading in the low-angle cross-bedded sandstones (Sl(e)). (B)

Inversely graded laminae in the large-scale trough cross-bedded sandstones (St(e)). (C) and (D) Distinct poikilotopic calcite cementation in the aeolian sandstones. Cal, calcite.

Fig. 10. (A) and (B) Inversely graded aeolian grainflow strata in the large-scale trough cross-bedded sandstones (St(e)). (C) and (D) Massive grainflow deposits bounded by pin-stripe lamination (white arrows) in the trough cross-bedded sandstones (St(e)).

Fig. 11. (A) Large-scaletrough cross-bedded sandstones (St(e)) interbedded with low-angle cross-bedded cobble to pebble conglomerates (Gch). (B) Close-up of (A). Distinct grainflow strata (gf) can be observed in the trough cross-bedded sandstones (St(e)). (C) Matrix-supported conglomerates (Gmd) are interbedded with trough cross-bedded sandstones (St(e)). Normal grading occurs in the conglomerates. These trough cross-bedded sandstones (St(e)) are bounded by flat sand-drift surfaces and flood surfaces. (D) Granule lags develop along the bounding surface. (E) Close-up of (D). (F) Scattered pebbles occur in the toesets of aeolian dune cross-strata.Scale: the geologist is 1.7 m long; the diameter of the camera lens cap is 7.7 cm.

Fig. 12. (A) Field photograph and (B) line drawing oflarge-scale trough cross-bedded sandstones (St(e)) interbedded with low-angle cross-bedded cobble to pebble conglomerates (Gch). Aeolian pods (remnants of aeolian dunes) show sharp contact, a flat base (sand-drift surface) and an erosional topsurface (upper erosive flood surface). Superimposition and reactivation surfaces are developed in the trough cross-bedded sandstones (St(e)). Geologist for scale is 1.7 m tall.

Fig. 13. (A)Field photograph and (B) line drawing oflarge-scale trough cross-bedded sandstones (St(e)) intercalated with matrix-supportedcobble to pebble conglomerates

(Gmd). Lenticular muddy sandstones (Ss) interfinger with the toeset of the overlying trough cross-bedded sandstones (St(e)). Superimposition and reactivation surfaces in the trough cross-bedded sandstones (St(e)) are abundant. These aeolian dune deposits are bounded by sand-drift and flood surfaces. Geologist for scale is 1.7 m tall.

Fig. 14. (A) Large-scale trough cross-bedded sandstones (St(e)) interbedded with low-angle cross-bedded cobbleto pebble conglomerates (Gch). Reactivation surfaces in the aeolian dune cross-strata are dominant. (B) Close-up of (A). Lenticular sandstones (Ss) show an intertonguing withthe toeset of the overlying trough cross-bedded sandstones (St(e)). Geologist for scale is 1.7 m tall.

Fig. 15. (A) Large-scale trough cross-bedded sandstones (St(e)) are covered by thick low-angle cross-bedded cobble to pebble conglomerates (Gch). Aeolian pods are preserved in the water-lain sandy conglomerates. (B) and (C) Alternating very fine-grained sandstones (Sm) and silty mudstones (Fl) show an intertonguing with the toeset of the overlying aeolian dune cross-strata. (D) and (E) Mud gravels and pebble and cobble deflation lags occur at the base of the overlying trough cross-bedded sandstones (St(e)). The hammer is 38 cm long.

Fig. 16. Depositional model of the aeolian desert system for the Chaling Basin during deposition of the Daijiaping Formation. Spatial and temporal distribution of different facies associations is shown. Based on the analysis of these facies associations, alluvial system (A), dry aeolian system (B) and wet aeoliansystem (C) are identified.

Fig. 17. Stratigraphic model accounting for the facies succession and surface development in the aeolian–fluvial unit of the Daijiaping Formation. Variations in

aridity degree, sand supply and water table are indicated on the right.

Fig. 18. Correlation between facies associations, depositional surfaces, water table oscillations and basin subsidence in the fluvial–aleolian unit (cf. Scherer and Lavina, 2005; Jones et al., 2016). The alternating aeolian and fluvial deposits and the development of sand-drift and flood surfaces are interpreted as high-frequency fluctuations of the water table and sediment supply driven by climate change. The long-term relative water-table rise is associated with basin subsidence.

Fig. 19. Schematic geological map showing the spatial distribution of aeolian deposits, evaporites and calcretes in the Upper Cretaceous (Coniacian to Maastrichtian) terrestrial red beds in East Asia (modified from Xi et al., 2019; Tan et al., 2020; Wu et al., 2022). The location of coastal mountains refers to Tan et al. (2020). Jl, Jiayin Basin; Hl, Hailar Basin; Sl, Songliao Basin; El, Erlian Basin; Gb, Gobi Basin; Zg, Junggar Basin; Th, Tuha Basin; Kq, Kuqa Basin; Tr,Tarim Basin ; Zl, Zoulang Basin; Jq, Jiuquan Basin; Xn-Lz, Xining-Lanzhou Basin; Or, Ordos Basin; Jl, Jiaolai Basin; Nh, Nanhua Basin; Hf, Heifei Basin; Sb, Subei Basin; Sc, Sichuan Basin; Js, Jianshi Basin; Jh, Jianghan Basin; Xj, Xinjiang Basin; Ym, Yuanma Bain; Hy, Hengyang Basin; Cl, Chaling Basin; Jt, Jitai Basin; Gz, Ganzhou Basin; Hc, Huichang Basin; Nx, Nanxiong Basin; Dx, Danxia Basin, Ss, Sanshui Basin; Cx, Chuxiong Basin; Lp-Sm, Lanping-Simao Basin.

Table captions

Table 1 Cretaceousstratigraphic sequences of the Chaling Basin, South China. The subdivision of the Stage of the Upper Cretaceous is based on the study of Xi et al. (2019). The dashed line indicates a paraconformity. The shaded region indicates the stratigraphic succession examined as part of this study.

Table 2 Summary of lithofacies observed in the Daijiaping Formation.

Table 3 Facies associations identified in the Daijiaping Formation.

Table 4 Classification, feature and interpretation of ancient aeolian–fluvial interaction types.

Figure captions

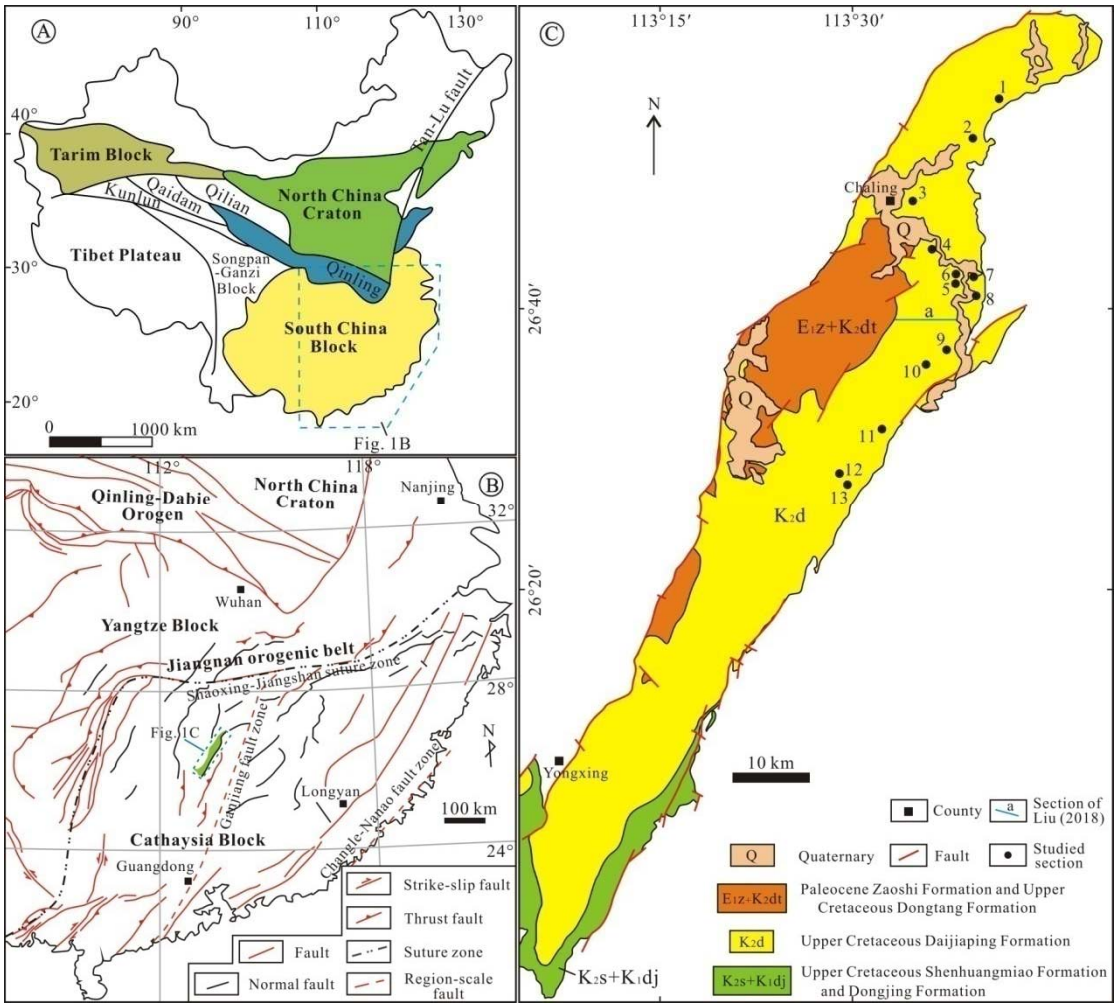

Fig. 1. (A) Sketch map of tectonic units in China showing the location of the South China Block (Li et al., 2014a). (B) Simplified geological map of South China depicting the distribution of Cretaceous Chaling basin (Li et al., 2014a). (C) Geological map of Chaling Basin. The locations of the studied outcrop sections are indicated.

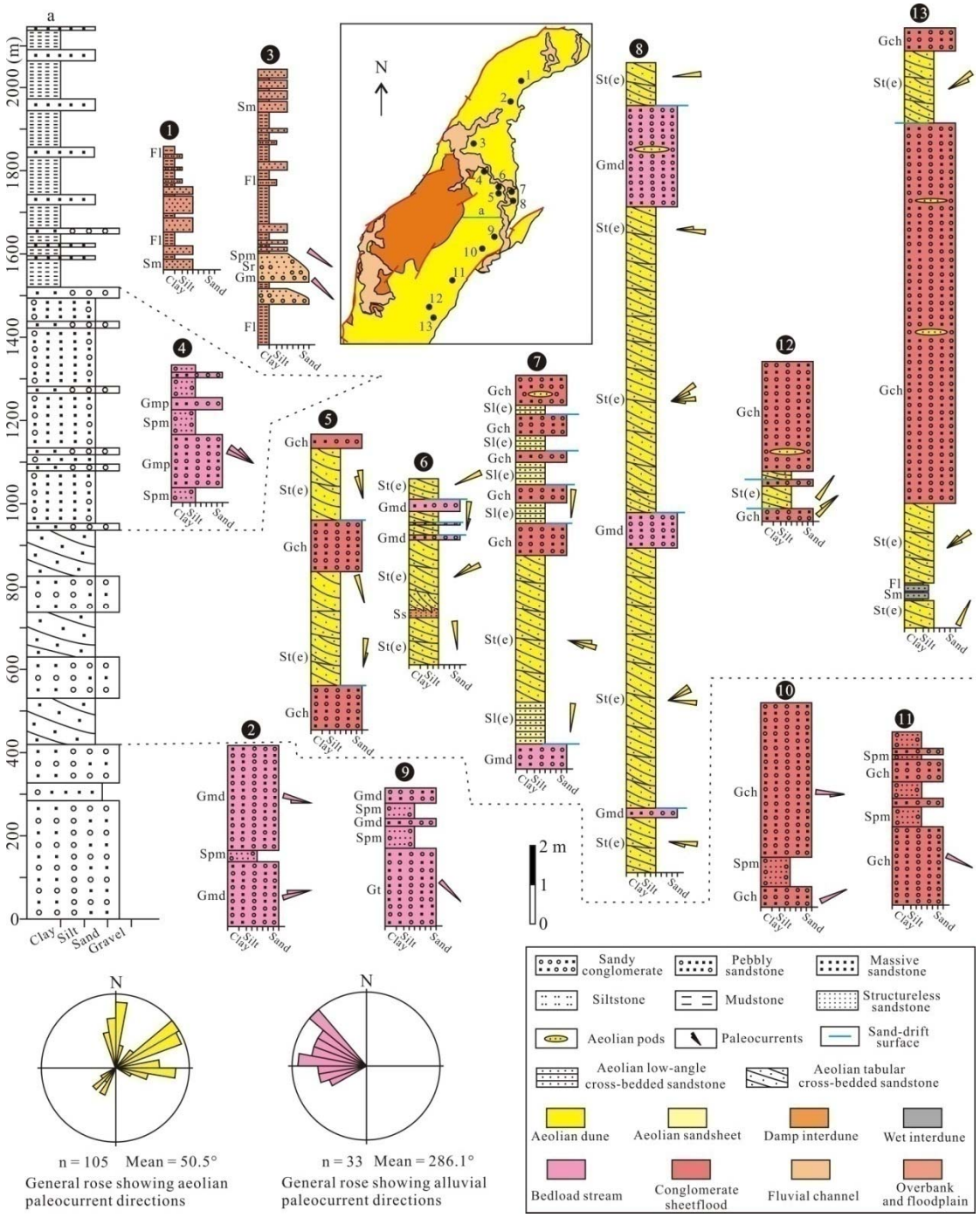

Fig. 2. Simplified sedimentary logs of the outcrop sections of the Daijiaping Formation showing the pattern of the paleocurrents. The locations of these sections are shown in Fig. 1C. Section a is modified from Liu (2018). See Table 2 for lithofacies codes.

Fig. 3. (A) and (B) Massive matrix to clast-supported cobble to pebble conglomerates (Gmd) bounded by concave-up erosive surfaces. (C) Trough cross-bedded conglomerates (Gct) with distinct pebble- to cobble-clast imbrication. (D) Clast-supported, trough cross-bedded cobble to pebble conglomerates overlain by pebbly sandstones (Spm). (E) Alternating matrix-supported fine pebble to granule conglomerates (Gmp) and pebbly sandstones (Spm) forming a fining-upward cycle. (F) Matrix-supported fine pebble to granule conglomerates (Gmp) interbedded with planar cross-bedded sandstones (Spx). Scale: The diameter of the camera lens cap is 7.7 cm; the hammer is 38 cm long; the field notebook is 18.2 long and 12.5 wide; the geologist is 1.7 cm tall.

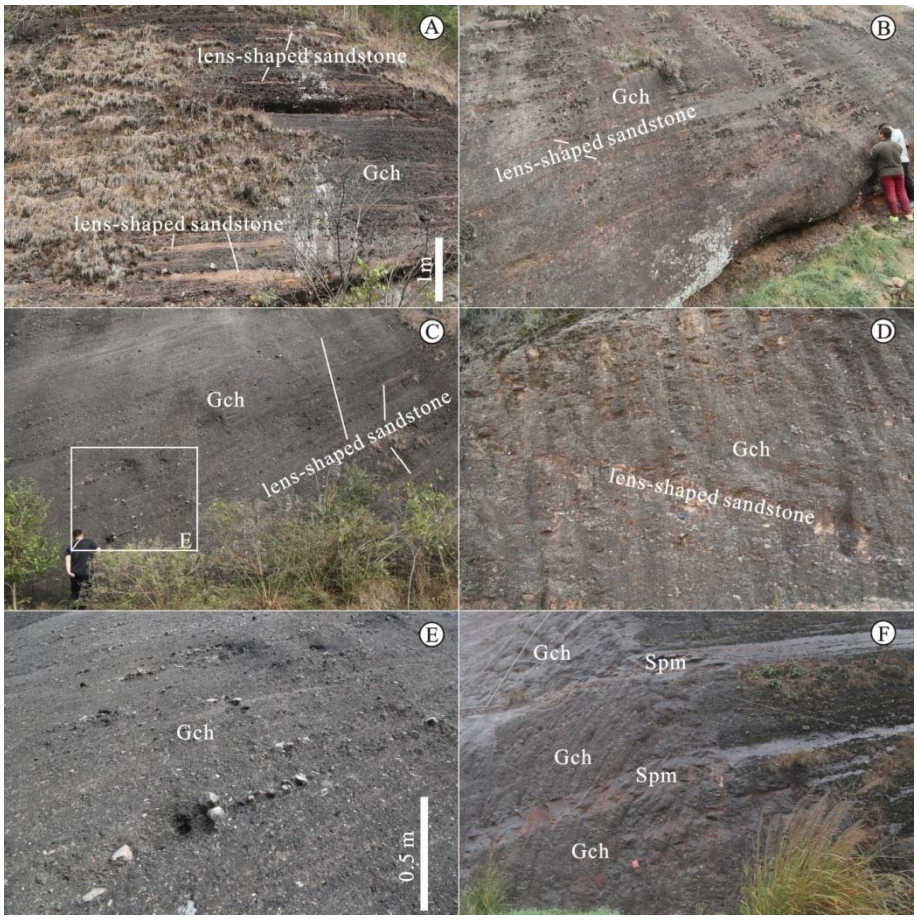

Fig. 4. (A) and (B) Clast-supported, horizontal to low-angle cross-bedded cobble to pebble conglomerates (Gch) with embedded lenticular sandstones. The geologist is 1.7 cm tall. (C) and (D) Planar cross-bedded conglomerates (Gch) containing lens-shaped sandstones. The geologist is 1.8 cm tall. (E) Close-up of (C). (F) Planar cross-bedded conglomerates (Gch) are interbedded with pebbly sandstones (Spm). The field notebook is 18.2 long and 12.5 wide.

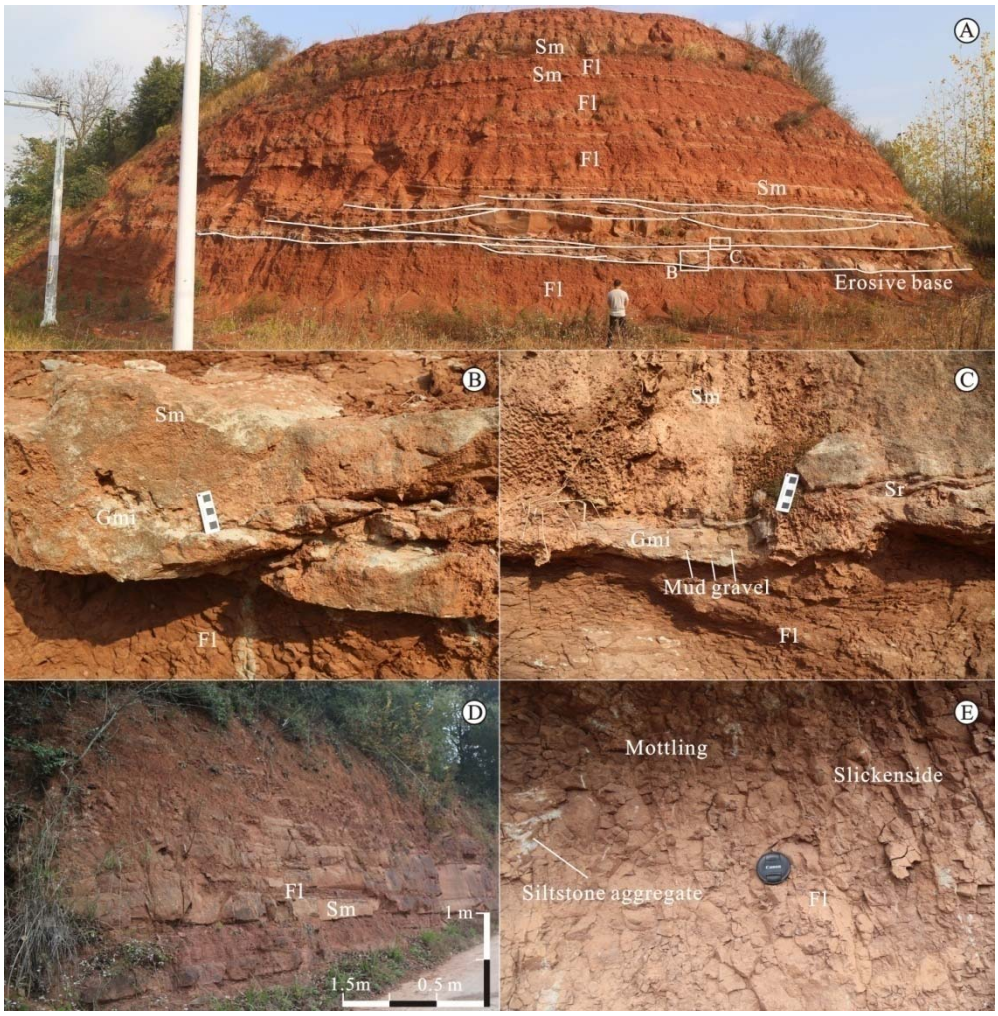

1416

1417 **Fig. 5.** (A) Thick silty mudstones (Fl) overlain matrix-supported conglomerates (Gmi),
1418 ripple cross-bedded sandstones (Sr), tabular sandstones (Sm) and lenticular or
1419 laminated silty mudstones (Fl) in ascending order. Interbedded tabular sandstones (Sm)
1420 and laminated silty mudstones (Fl) develop at the top of the outcrop section. Geologist
1421 for scale is 1.7 m tall. (B) and (C) Close-up of (A). Purple mudstone intraclasts occur
1422 in the conglomerates. (D) Alternating tabular sandstones (Sm) and laminated silty
1423 mudstones (Fl). (E) Close-up of thick silty mudstones showing pale grey-green mottling,
1424 slickensides and siltstone aggregates. The diameter of the camera lens cap is 7.7 cm.

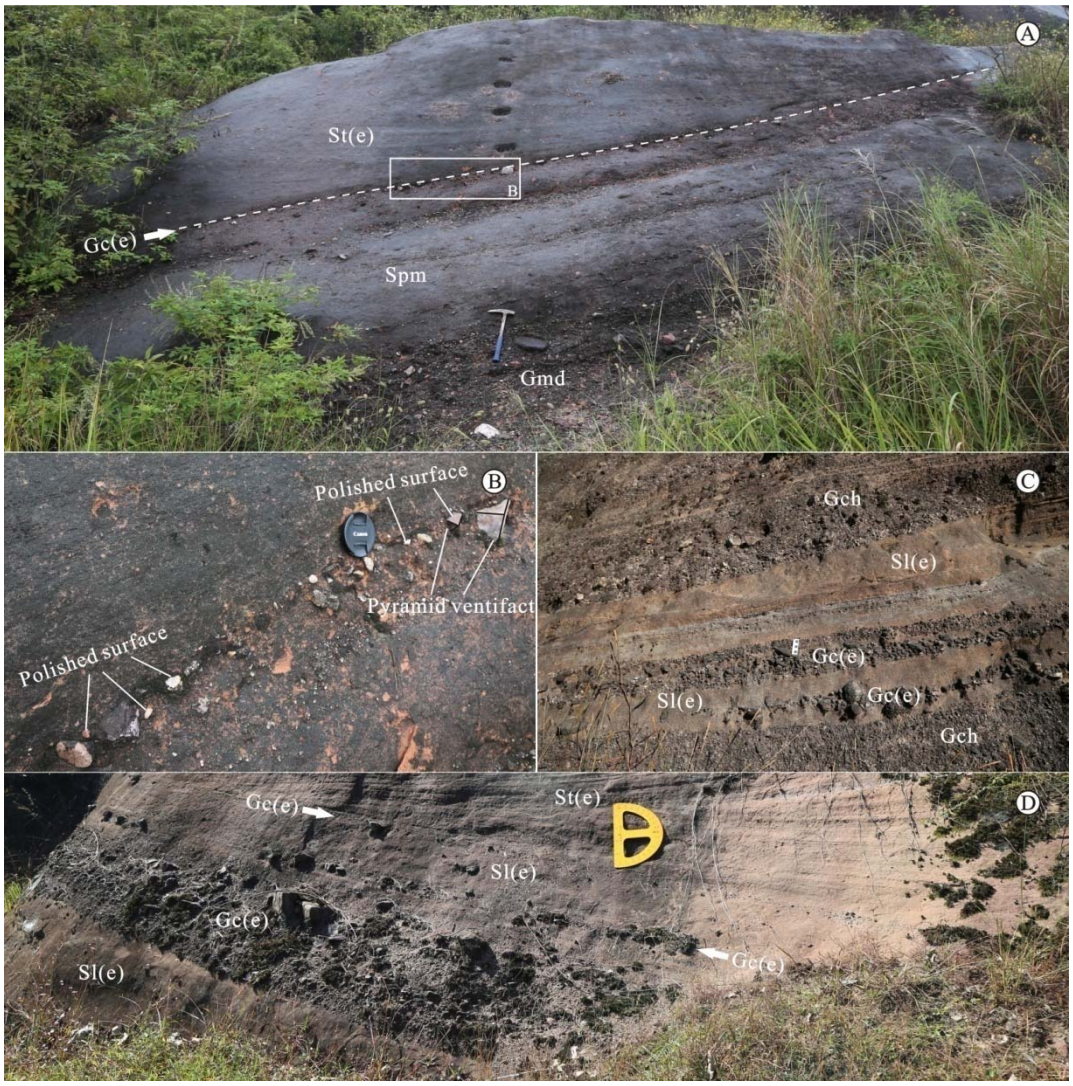

Fig. 6. (A) Laterally continuous quartzite pebbles (Gc(e)) overlain by large-scale tabular cross-bedded sandstones (St(e)). (B) Close-up of quartzite pebbles. These pebbles show polished surfaces and pyramid shapes. (C) Tabular clast-supported conglomerates (Gc(e)) are interbedded with low-angle cross-bedded sandstones (Sl(e)). (D) Tabular clast-supported conglomerates (Gc(e)) with flat base and top surfaces overlain by low-angle cross-bedded sandstones (Sl(e)). Scale: the hammer is 38 cm long; the diameter of the camera lens cap is 7.7 cm.

1433

1434 **Fig. 7.** (A) Low-angle cross-bedded sandstones (Sl(e)) overlain by large-scale trough

1435 cross-bedded sandstones (St(e)). (B) and (C) Laterally continuous limestones and

1436 quartzite pebbles (Gc(e)) overlain by low-angle cross-bedded sandstones (Sl(e)). (D)

1437 Isolated occurrence of sub-horizontal laminated sandstones (Sl(e)). (E) Close-up of (D)

1438 showing the alternation of lags of granules (gr) and wind-ripple deposits (wr). Geologist

1439 for scale is 1.7 m tall.

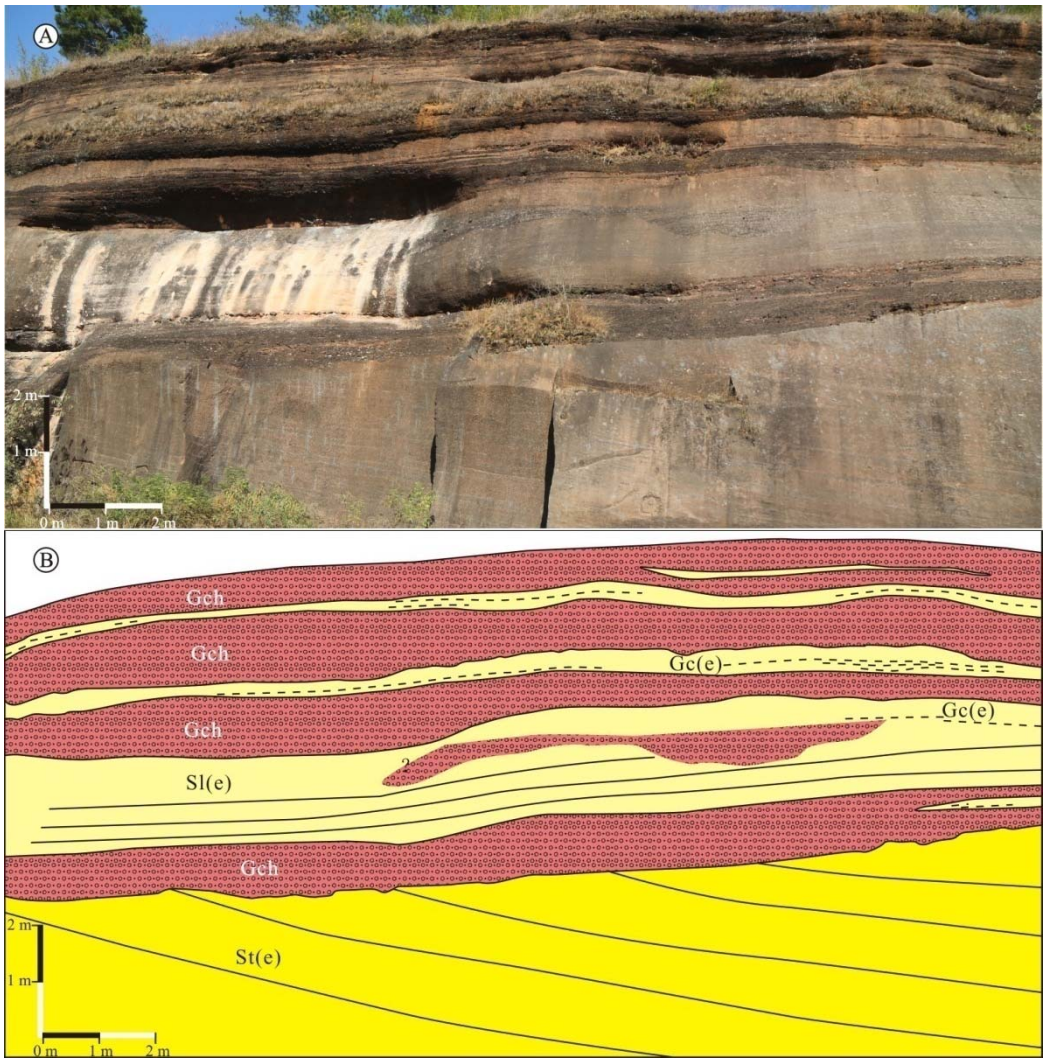

1440

1441 **Fig. 8.** (A) Field photograph and (B) line drawing of low-angle cross-bedded sandstones

1442 (Sl(e)) interbedded with horizontal to low-angle cross-bedded conglomerates (Gch).

1443 Discrete pebbles (Gc(e)) pinch out laterally in the low-angle cross-bedded sandstones

1444 (Sl(e)).

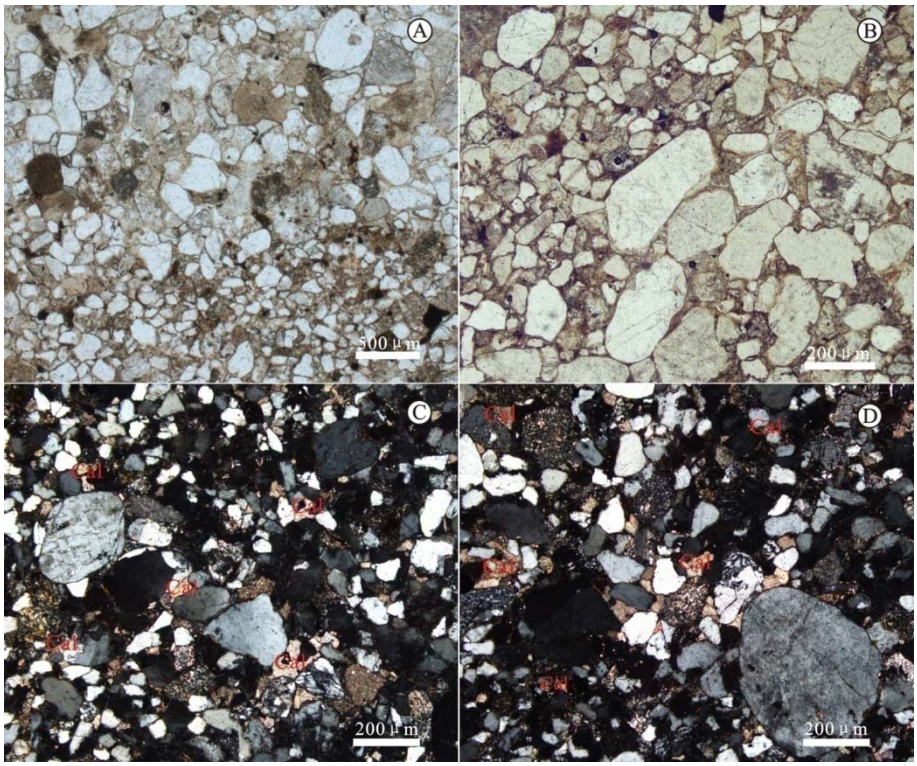

Fig. 9. (A) Inverse grading in the low-angle cross-bedded sandstones (Sl(e)). (B) Inversely graded laminae in the large-scale trough cross-bedded sandstones (St(e)). (C) and (D) Distinct poikilotopic calcite cementation in the aeolian sandstones. Cal, calcite.

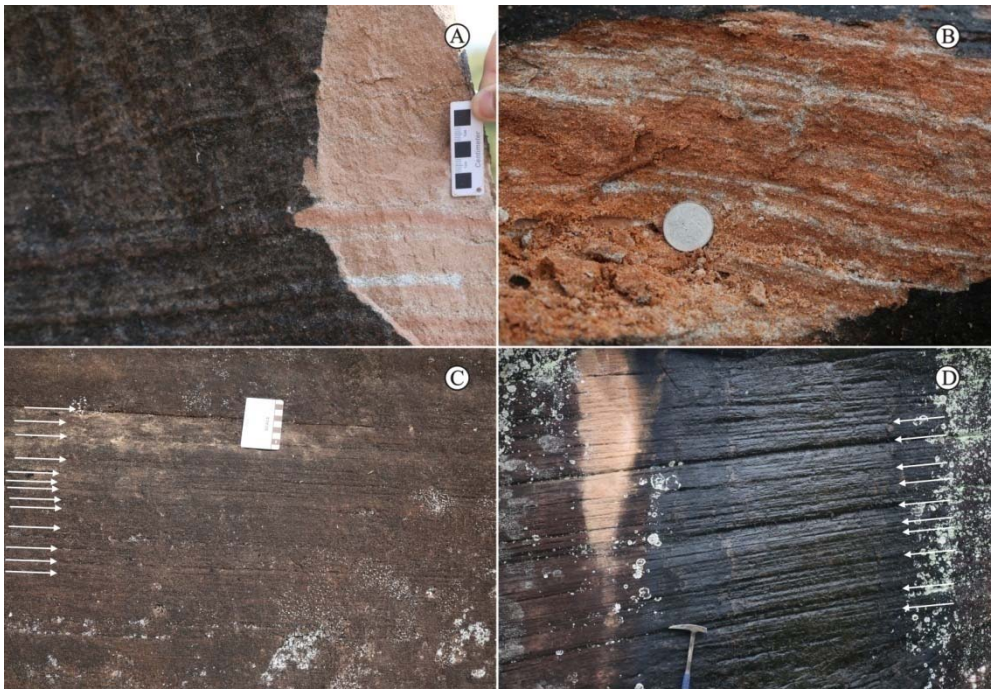

Fig. 10. (A) and (B) Inversely graded aeolian grainflow strata in the large-scale trough

cross-bedded sandstones (St(e)). (C) and (D) Massive grainflow deposits bounded by pin-stripe lamination (white arrows) in the trough cross-bedded sandstones (St(e)).

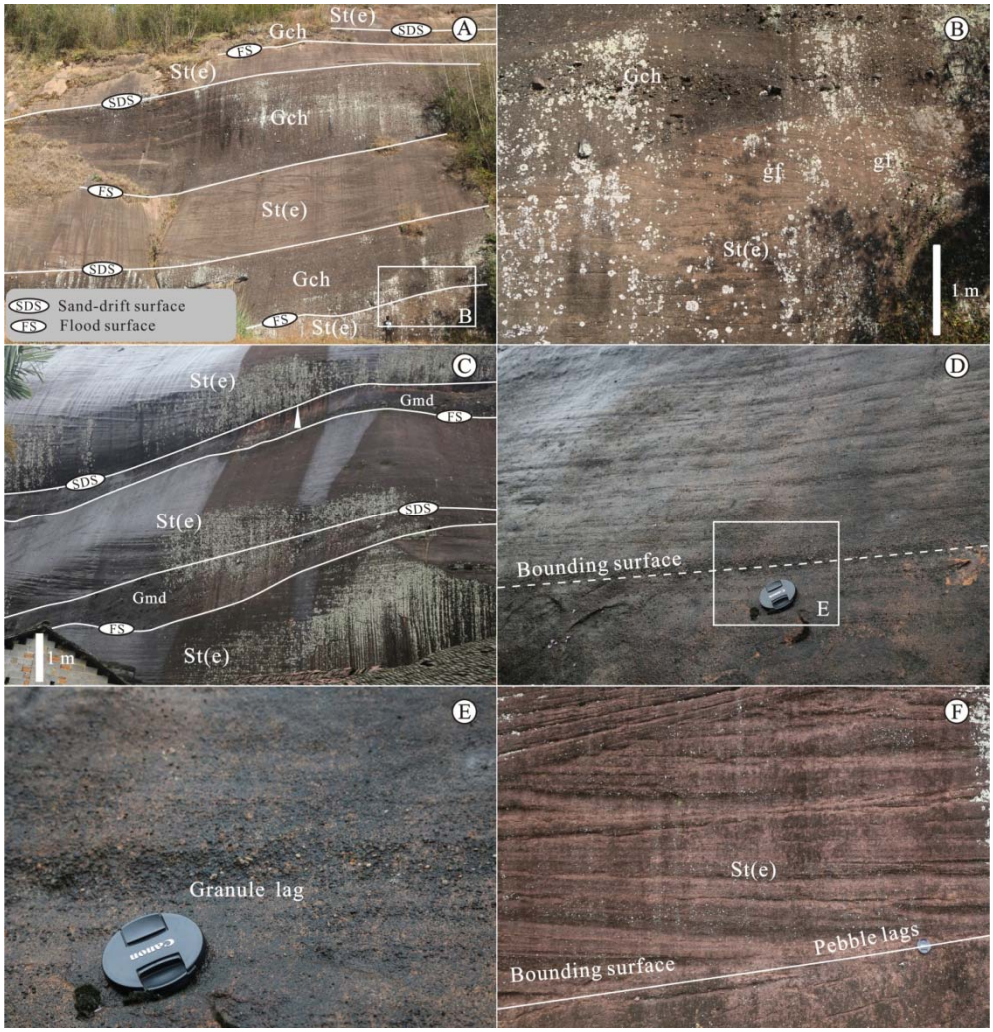

Fig. 11. (A) Large-scaletrough cross-bedded sandstones (St(e)) interbedded with low-angle cross-bedded cobble to pebble conglomerates (Gch). (B) Close-up of (A). Distinct grainflow strata (gf) can be observed in the trough cross-bedded sandstones (St(e)). (C) Matrix-supported conglomerates (Gmd) are interbedded with trough cross-bedded sandstones (St(e)). Normal grading occurs in the conglomerates. These trough cross-bedded sandstones (St(e)) are bounded by flat sand-drift surfaces and flood surfaces. (D) Granule lags develop along the bounding surface. (E) Close-up of (D). (F) Scattered pebbles occur in the toesets of aeolian dune cross-strata.Scale: the geologist is 1.7 m

1462 long; the diameter of the camera lens cap is 7.7 cm.

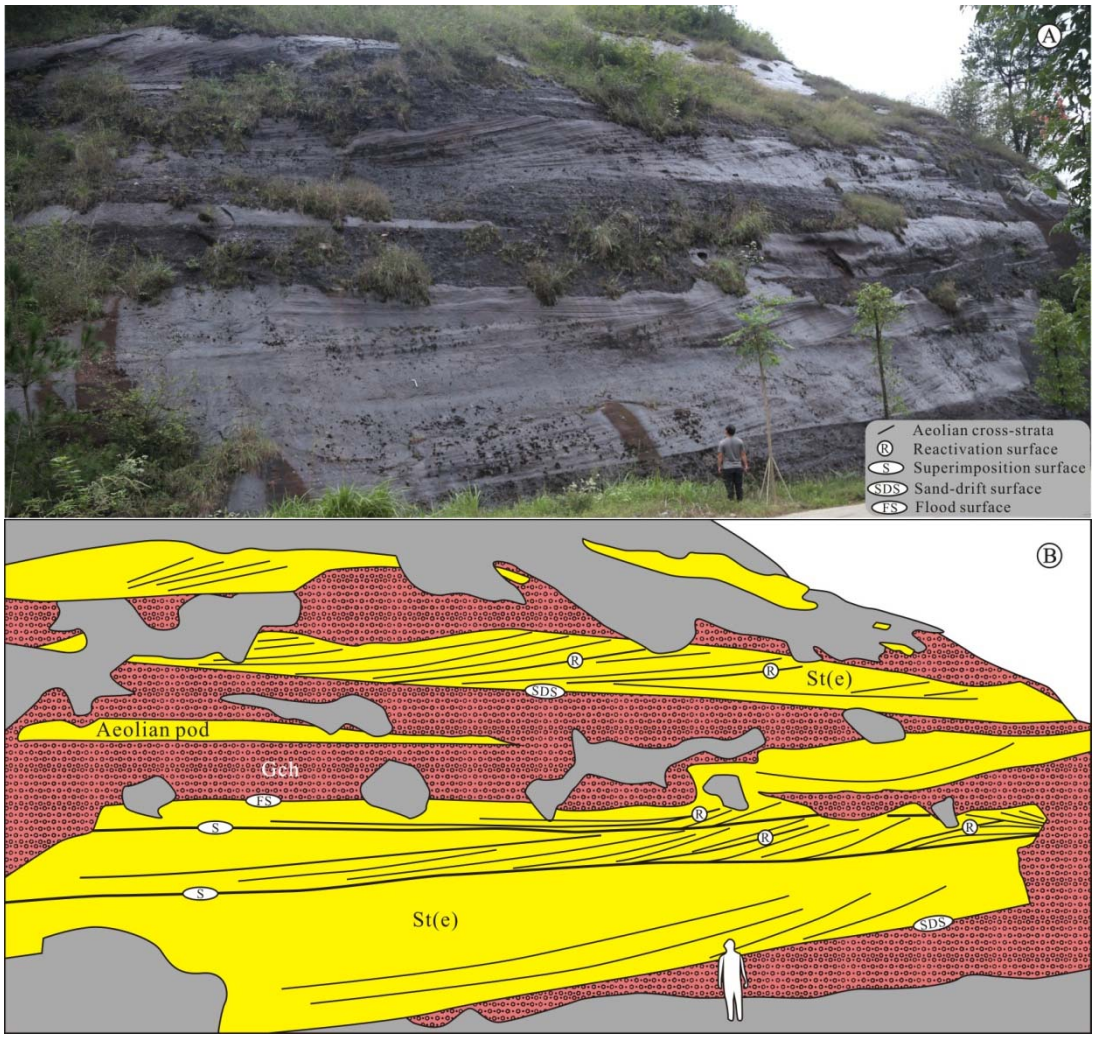

1463

1464 **Fig. 12.** (A) Field photograph and (B) line drawing oflarge-scale trough cross-bedded

1465 sandstones (St(e)) interbedded with low-angle cross-bedded cobble to pebble

1466 conglomerates (Gch). Aeolian pods (remnants of aeolian dunes) show sharp contact, a

1467 flat base (sand-drift surface) and an erosional topsurface (upper erosive flood surface).

1468 Superimposition and reactivation surfaces are developed in the trough cross-bedded

1469 sandstones (St(e)). Geologist for scale is 1.7 m tall.

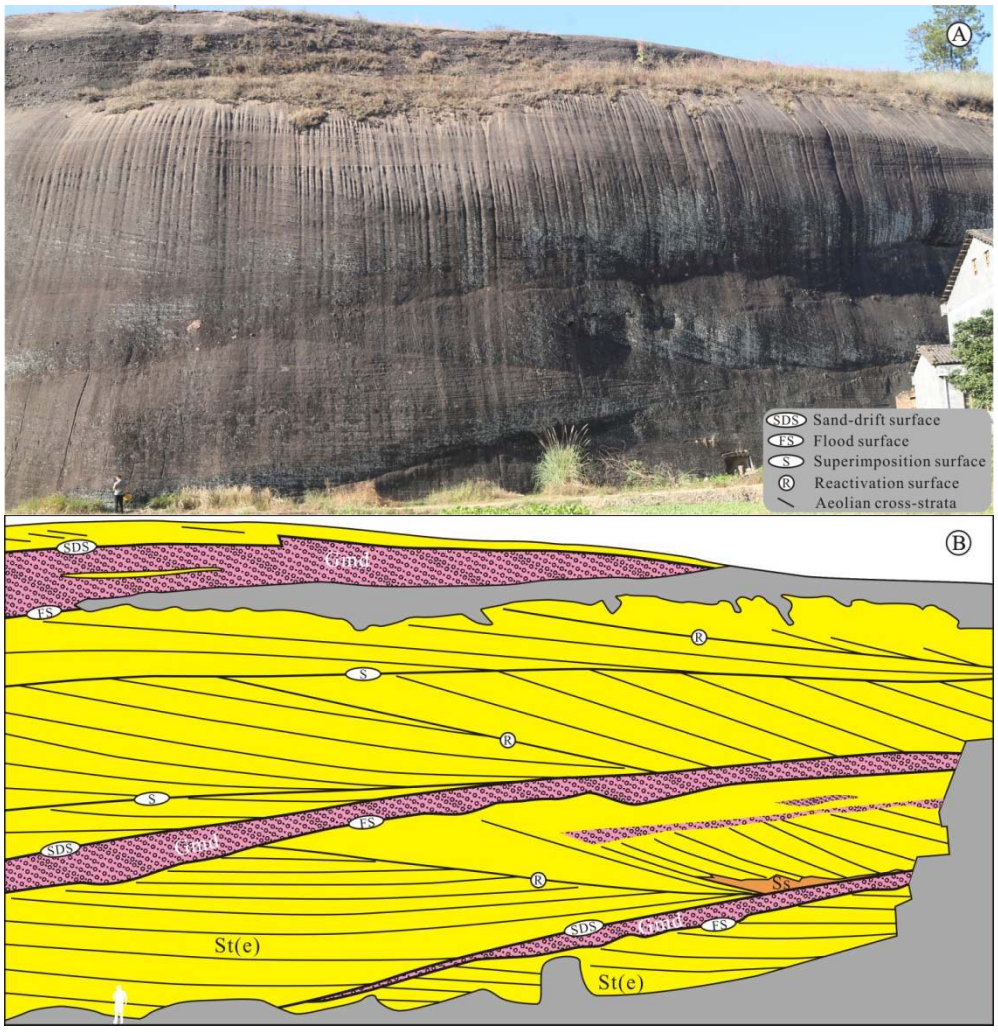

Fig. 13. (A)Field photograph and (B) line drawing oflarge-scale trough cross-bedded sandstones (St(e)) intercalated with matrix-supportedcobble to pebble conglomerates (Gmd). Lenticular muddy sandstones (Ss) interfinger with the toeset of the overlying trough cross-bedded sandstones (St(e)). Superimposition and reactivation surfaces in the trough cross-bedded sandstones (St(e)) are abundant. These aeolian dune deposits are bounded by sand-drift and flood surfaces. Geologist for scale is 1.7 m tall.

1477

1478 **Fig. 14.** (A) Large-scale trough cross-bedded sandstones (St(e)) interbedded with low-

1479 angle cross-bedded cobbleto pebble conglomerates (Gch). Reactivation surfaces in the

1480 aeolian dune cross-strata are dominant. (B) Close-up of (A). Lenticular sandstones (Ss)

1481 show an intertonguing withthe toeset of the overlying trough cross-bedded sandstones

1482 (St(e)). Geologist for scale is 1.7 m tall.

1483

1484 **Fig. 15.** (A) Large-scale trough cross-bedded sandstones (St(e)) are covered by thick
1485 low-angle cross-bedded cobble to pebble conglomerates (Gch). Aeolian pods are
1486 preserved in the water-lain sandy conglomerates. (B) and (C) Alternating very fine-
1487 grained sandstones (Sm) and silty mudstones (Fl) show an intertonguing with the toeset
1488 of the overlying aeolian dune cross-strata. (D) and (E) Mud gravels and pebble and
1489 cobble deflation lags occur at the base of the overlying trough cross-bedded sandstones
1490 (St(e)). The hammer is 38 cm long.

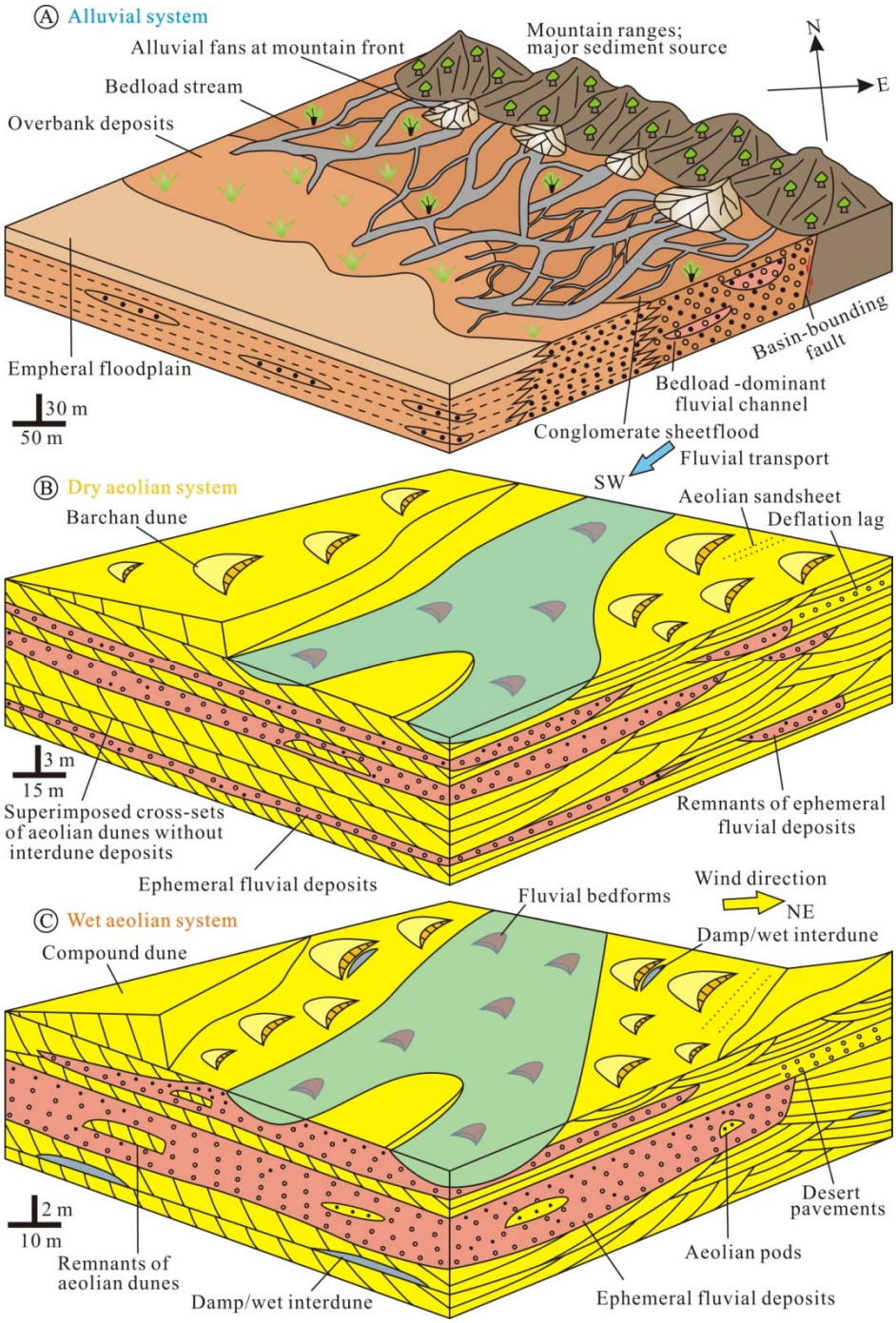

1491

1492 **Fig. 16.** Depositional model of the aeolian desert system for the Chaling Basin during

1493 deposition of the Daijiaping Formation. Spatial and temporal distribution of different

1494 facies associations is shown. Based on the analysis of these facies associations, alluvial

1495 system (A), dry aeolian system (B) and wet aeoliansystem (C) are identified.

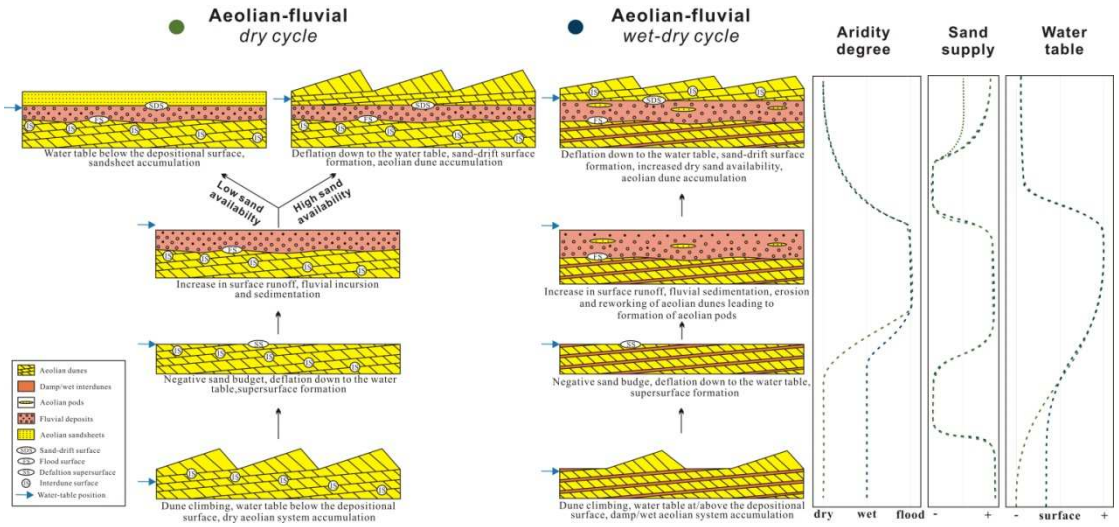

Fig. 17. Stratigraphic model accounting for the facies succession and surface development in the aeolian–fluvial unit of the Daijiaping Formation. Variations in aridity degree, sand supply and water table are indicated on the right.

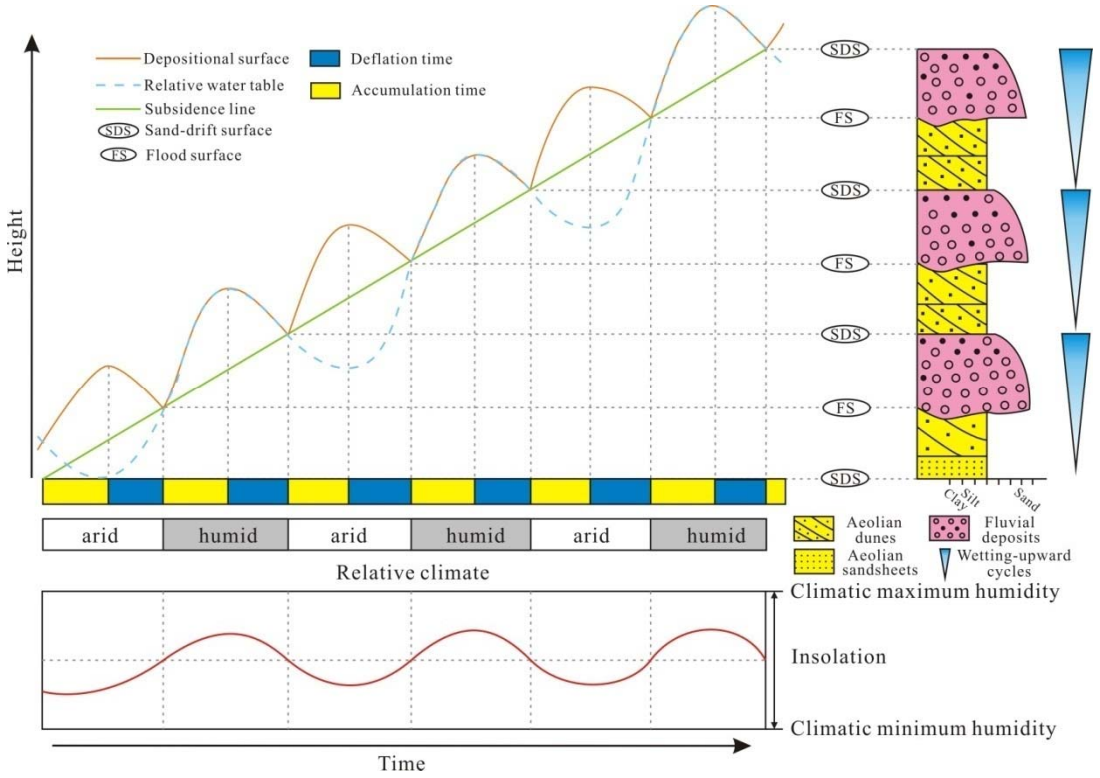

Fig. 18. Correlation between facies associations, depositional surfaces, water table oscillations and basin subsidence in the fluvial–aleolian unit (cf. Scherer and Lavina, 2005; Jones et al., 2016). The alternating aeolian and fluvial deposits and the

development of sand-drift and flood surfaces are interpreted as high-frequency fluctuations of the water table and sediment supply driven by climate change. The long-term relative water-table rise is associated with basin subsidence.

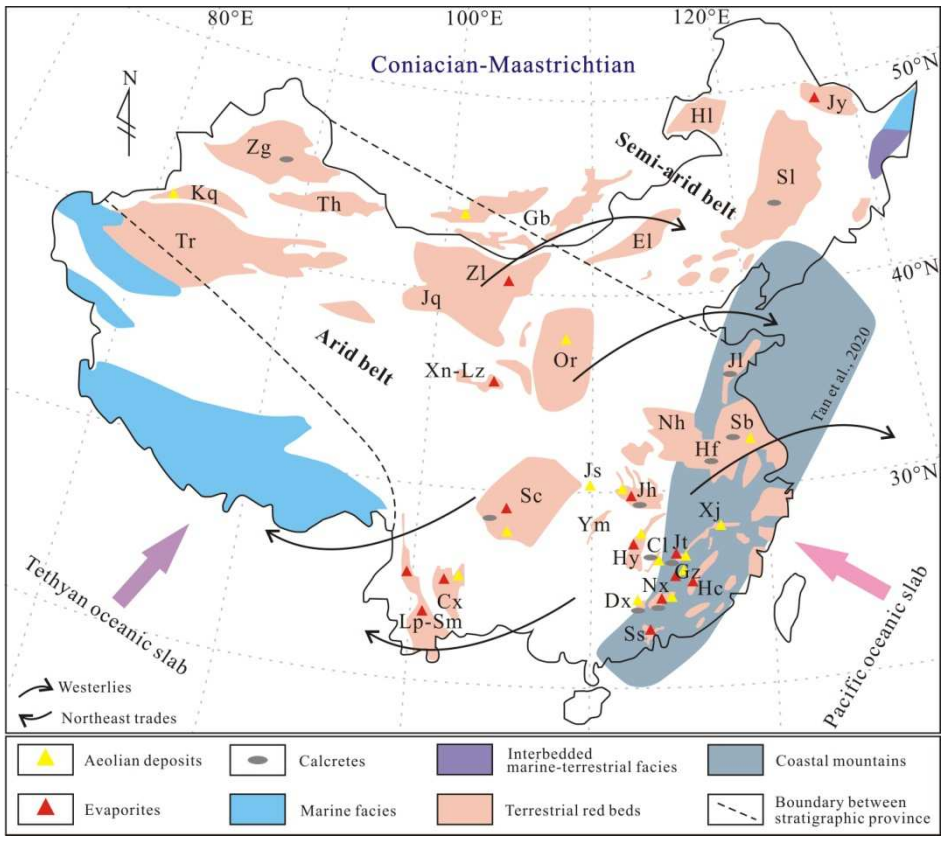

Fig. 19. Schematic geological map showing the spatial distribution of aeolian deposits, evaporites and calcretes in the Upper Cretaceous (Coniacian to Maastrichtian) terrestrial red beds in East Asia (modified from Xi et al., 2019; Tan et al., 2020; Wu et al., 2022). The location of coastal mountains refers to Tan et al. (2020). Jl, Jiayin Basin; Hl, Hailar Basin; Sl, Songliao Basin; El, Erlian Basin; Gb, Gobi Basin; Zg, Junggar Basin; Th, Tuha Basin; Kq, Kuqa Basin; Tr,Tarim Basin ; Zl, Zoulang Basin; Jq, Jiuquan Basin; Xn-Lz, Xining-Lanzhou Basin; Or, Ordos Basin; Jl, Jiaolai Basin; Nh, Nanhua Basin; Hf, Heifei Basin; Sb, Subei Basin; Sc, Sichuan Basin; Js, Jianshi Basin; Jh, Jianghan Basin; Xj, Xinjiang Basin; Ym, Yuanma Bain; Hy, Hengyang Basin; Cl,

Chaling Basin; Jt, Jitai Basin; Gz, Ganzhou Basin; Hc, Huichang Basin; Nx, Nanxiong Basin; Dx, Danxia Basin, Ss, Sanshui Basin; Cx, Chuxiong Basin; Lp-Sm, Lanping-Simao Basin.

Table captions

Table 1 Cretaceousstratigraphic sequences of the Chaling Basin, South China. The subdivision of the Stage of the Upper Cretaceous is based on the study of Xi et al. (2019). The dashed line indicates a paraconformity. The shaded region indicates the stratigraphic succession examined as part of this study.

Series	Formation	Unit	Stage	Thickness (m)	Lithology	Facies association	Climate
Upper Cretaceous	Dongtang	K_2dt	Maastrichtian	779	Sandstone, siltstone and silty mudstone with conglomerate	Fluvial deposits	wet
	Daijiaping	K_2d	Campanian-Maastrichtian	2356	Conglomerate, quartz sandstone , siltstone and mudstone	Aeolian–fluvial deposits	dry
	Shenhuang shan	K_2s	Cenomanian-Campanian	1116	Muddy siltstone and silty mudstonewith conglomerate	Fluvial and lacustrine deposits	wet
Lower Cretaceous	Dongjing	K_1dj	Aptian-Albian	135–478	Conglomerate and sandy conglomerate with silty mudstone	Alluvial fan	wet

1547 **Table 2** Summary of lithofacies observed in the Daijiaping Formation.

Facies code	Description	Interpretation
Gmd	Matrix to clast-supported, disorganized to poorly organized cobble and pebble conglomerate, subrounded to rounded, poorly sorted, granule to sand matrix, weak imbrication, erosional base, sheet-like or wedge-shaped units	Hyperconcentrated flood flow with high sediment load
Gmp	Matrix-supported, disorganized to moderately organized fine pebble and granule conglomerate, sand matrix, subrounded to rounded, moderately to well-sorted, weak imbrication, crudely stratified, ungraded or normally graded, erosional or irregular base, sheet-like units	Deposits of gravel sheets emplaced by high-magnitude flood flows.
Gmi	Matrix-supported, disorganized fine pebble and granule conglomerate with mud intraclasts, sand matrix, poorly sorted, subrounded to rounded, low-relief scouring base, overlain by ripple cross-bedded sandstone (Sr)	Channel lags caused by erosion of the basal channel or by channel bank collapse
Gct	Clast-supported, trough cross-bedded cobble and pebble conglomerate, granule to sand matrix, subrounded to rounded, normally graded, imbrication, sharp and low-relief scouring base	Migration of gravel bars with well-developed slipfaces
Gch	Clast-supported, planar or horizontal to low-angle cross-bedded cobble and pebble conglomerate, alternation of coarse and finer gravel or gravel-rich and sand-rich strata, subrounded to rounded, normally graded, imbrication, sheet-like units	Sediment-charged, upper-flow regime sheetflood
Gc(e)	Discrete limestone and quartzite pebbles and cobbles or decimeter-thicktabular clast-supported conglomerates with matrix of sand and granule, flat base and top surfaces	Long-lasting wind deflation of water-lain deposits and stacking of deflation lags.
St(e)	Very fine- to fine sandstone, well to very well-sorted, large-scale trough cross-bedding, presence of reactivation and superimposition surfaces, several meter to decameter-thick cross-sets formed by inversely graded foresets	Migration and climbing of aeolian dunes.
Sl(e)	Fine- to coarse sandstones, well-sorted, centimeter to several meter-thick tabular units, horizontal bedding or low angle cross-bedding, inverse grading	Migration and subcritical climbing of wind ripples on dry depositional surfaces.
Ss	Structureless sandstones arranged in lens-shape beds,an intertonguing with the toeset of the overlying trough cross-stratified sandstone	Deposition on a damp bounding surface where the capillary fringe of the groundwater level reached

		the depositional surface.
Spx	Fine sandstone, crudely planar cross-bedding, meter-thick tabular units, interbedded with matrix-supported fine pebble conglomerate (Gmp)	Migration of channel sand bars with well-developed slipfaces
Sr	Fine-grained sandstone, ripple cross-bedding, centimeter-thick lamination	Migration of ripple-scale bedforms
Spm	Fine sandstone (scattered pebbles), poorly to moderately sorted, presence of small pebbles, interbedded with matrix-supported small pebble conglomerate (Gmp) or clast-supported cobble and pebble conglomerate (Gmd)	Rapid deposition from sand-laden flows during waning flows
Sm	very fine- to fine massive sandstone, moderatelysorted, decimeter-thick tabular units	Rapid deposition form subaqueous high-energy flows
Fl	Purple laminated or massive silty mudstones, irregular mottles, pedogenic slickensides	Deposition of suspended load in standing water

Table 3 Facies associations identified in the Daijiaping Formation.

Facies associations	Lithofacies types	Sedimentary structures and geometry
FA-1: Bedload streamflow deposits	Gmd, Gmp, Gct, Spm, Spx	Tabular body or lens-shaped units with sharp erosive bases, fining-upward units
FA-2: Sheetflood deposits	Gch	Tabular intervals with flat orlow-relief bases, normally graded
FA-3: Meandering fluvial channel deposits	Gmi, Sr, Sm, Fl	Fining-upward units, decameter-thicktabular bodies with concave-up erosional bases
FA-4: Overbank flood and floodplain deposits	Sm, Fl	Fining-upward cycles, non-erosional bases
FA-5: Deflation lags/ Desert pavements	Gc(e)	Lineation of pebbles and cobbles or tabular bodies with ventifacts
FA-6: Aeolian sandsheet	Sl(e)	Inverse grading, wind-ripple lamination
FA-7: Aeolian dune	St(e)	Large-scale tangential tabular cross-strata, grainflow deposits
FA-8: Damp interdune	Ss	Structureless lenses
FA-9: Wet interdune	Sm, Fl	Tabular body, fining-upward cycles

1551 **Table 4** Classification, feature and interpretation of ancient aeolian–fluvial interaction types.

Interaction type	Stratigraphic units	Facies associations	Depositional feature and interpretation	Size of cycles	References
Short-term aeolian–fluvial interaction	The Proterozoic Mancheral Quartzite, Pranhita-Godavari Vally, India	Aeolian sandsheets, in-channel coarse lag deposits, braid bars and proximal floodplain.	Aeolian deposits developed in the distal floodplain or inter-channel area. Accumulation of aeolian deposits was controlled by the architecture of the fluvial system.	10–30 cm thick wind-ripple strata	Chakraborty and Chaudhuti, 1993
	The Middle Proterozoic Eriksfjord Formation, southwest Greenland	Stream and channel deposits, ephemeral flash floods and wind ripple laminae.	Aeolian deposits occurred as drapes or continuous beds within fluvial deposits. The preservation of aeolian deposits was optimal in fluvial systems formed in a humid climate.	A few centimeters to 0.4 m thick wind ripple laminae	Tirsgaard andØxnevad, 1998
	The Upper Silurian Tumblagooda Sandstone, western Australia	Aeolian sandsheets, small aeolian dunes, interdune ponds and braided fluvial deposits.	Mixed fluvial and aeolian sandsheet deposits were bounded by thick fluvial sandstones. Aeolian sandsheet deposits were dominated by the architecture of the fluvial system.	<2 m thick aeolian sandsheets and aeolian dunes	Trewin, 1993
	The Siluro-Devonian Swanshaw Sandstone Formation, SW Scotland	Aeolian sandsheets, small aeolian dunes, braided channels and floodplain, mudflat.	Aeolian deposits formed on the floodplain during dry periods. They were closely associated with the architecture of a semi-arid proximal alluvial plain.	0.02–0.1 m thick wind-ripple strata and 0.06–0.13 m thick aeolian dunes	Smith et al., 2006
	The Upper Cretaceous capping sandstone, Kaiparowits Basin, USA	Wind ripple laminae, small aeolian dunes and braided stream systems.	Aeolian deposits occurred as lamina at the top of fluvial bar deposits, and as small dunes located amid braided stream systems. The resulting change from fluvial to aeolian was a short-term shift to a more semi-arid to arid climate over a seasonal timeframe.	Thin wind-ripple strata and 0.3–1.2 m thick aeolian dunes	Simpson et al., 2008

Fluvial incursions into aeolian dune fields without elevated water-table level	The Upper Permian Dawlish Sandstone Formation, Wessex Basin, UK	Aeolian dunes, aeolian sandsheets and fluvial channels	The succession is represented by the alternating fluvial conglomerate and aeolian dune sandstone. The drying-wetting cycles developed. The variability of aeolian and fluvial sedimentary architecture was related to a local climatic change.	~2.6–6.2 m	Newell et al., 2001
	The Permian Brodick Beds, UK	Aeolian dunes, aeolian sandsheets, dry interdunes, fluvial and lacustrine deposits.	The wetting- and drying-upward cycles developed. The sedimentary cyclesreflected climatic oscillations.	~7–62 m	Clemmensen and Abrahamsen, 1983; Frederiksen et al., 1998
	The Upper Jurassic Sergi Formation, Recŏncavo Basin, Brazil	Lacustrine mudstones, aeolian dunes, aeolian sandsheets, ephemeral fluvial systems, braided channel belt deposits and sheetfloods.	The formation consists of three depositional sequences bounded by regional unconformities. The vertical changes between fluvial and aeolian depositional systems were caused by tectonic and climate factors.	~5–7 m	Scherer et al., 2007
	The Upper Jurassic Tianchihe Formation, Ningwu–Jingle Basin, China	Meandering fluvial channel, levee and overbank, aeolian dunes, aeolian sandsheets, ephemeral fluvial channel, floodplain.	Small-scale drying-wetting cycles occurred in the erg systems. The vertical changes from fluvial to aeolian deposits indicated a local variation from relatively humid to arid conditions.	~1.4–21.7 m	Xu et al., 2019
	The Upper Jurassic–Lower Cretaceous	Distal floodflows, ephemeral fluvial	The fluvial facies was intertongued with aeolian deposits. The wetting-upward cycles resulted	5–14 m	Scherer and Lavina, 2005,

	GuaráFormation of the Paraná Basin, southern Brazil and Batoví Member, Norte Basin, Uruguay	channels, perennial braided fluvial channels aeolian dunes and aeolian sandsheets.	from erg expansion and contraction probably triggered by climatic changes.		2006; Amarante et al., 2019; Reis et al., 2019, 2022
	The Lower CretaceousSão Sebastião Formation, JatobáBasin, Brazil	Aeolian dunes, aeolian sandsheets, sheet floods and ephemeral fluvial channels	Interactions between aeolian and fluvial systems are due to autocyclic influences related to seasonal climatic oscillations.	<4 m	Ferronatto et al., 2019
Fluvial incursions into aeolian dune fields associated with elevated groundwater levels	The Pennsylvanian Piauí Formation, Parnaíba Basin, Brazil	Aeolian dunes, aeolian sandsheets, dry to damp interdunes, fluvial channels, shoreface, shoreface-shelf transition, floodplains and lacustrine margin.	The formation recorded the deposition of aeolian, fluvial, lacustrine and shallow marine systems. The main controls on the sedimention were attributed to glacio-eustasy and climate.	<13 m	Vieira and Scherer, 2017; Kifumbi et al., 2022
	The Permian Cutler Group, Paradox Basin, USA	Aeolian dunes, aeolian sandsheets, wet interdunes, fluvial channels and sheetflood and overbank deposits.	Aeolian deposits occurred in the medial and distal parts of the succession. Fluvial deposits were intertongued with aeolian deposits. The drying-wetting cycles developed. Basin- and small-scale interaction types recorded region-wide, longer-term climatic variations and autocyclic flood events within the dune field, respectively.	<8 m (small-scale interaction types)	Langford and Chan, 1989; Mountney and Jagger, 2004; Jordan and Mountney, 2010; Cain and Mountney, 2011
	The Permian De La Cuesta Formation,	Aeolian dunes, dry and wet interdunes, aeolian	The formation is characterized by erg deposits interbedded with terminal alluvial fan deposits.	~2.5–37.5 m	Spalletti et al., 2010

Paganzo Basin, NW Argentina	sandsheets, mudflat and ephemeral fluvial deposits.	Alternating aeolian and ephemeral fluvial systems resulted from cyclical climatic changes.		
The Permian Upper Rotliegend Group, North Sea	Aeolian dunes, aeolian sandsheets, dry/wet indunes, ephemeral fluvial deposits and playa and lacustrine deposits.	The relative dominance of water and winddeposition in this formation was a function of fluctuations in the discharge of ephemeral fluvial systems and changes in water table/playa level driven by a combination of climatic change and syndepositional tectonics.	~10–50 m	Ellis, 1993; Sweet, 1999
The Triassic Helsby Sandstone Formation, UK	Aeolian dunes, dry/damp/wet indunes and minor fluvial channels	Downwind changes in the geometry and facies of the interdune units indicate periodic expansion and contraction of the interdunes in response to changes in the elevation of the groundwater table and episodic flooding.	<4 m	Mountney and Thompson,2002
The Triassic Ormskirk Sandstone, Irish Sea and UK	Aeolian dunes, aeolian sandsheets, damp interdunes and fluvial channels, sheetflood and overbank deposits	The small aeolian deposits developed within a dominantly fluvial setting. The drying-upward units recorded climate-controlled variations in the groundwater table and episodic flooding.	<6 m	Cowan, 1993; Herries and Cowan, 1997
The Lower Jurassic Kayenta and Navajo Sandstone formations, Colorado Plateau, USA	Aeolian dunes, aeolian sandsheets, dry, damp and wet interdunes and braided and ephemeral fluvial deposits.	Three distinct fluvial–aeolian cycles with many subordinated ones were recognized. These large-scale interaction types reflected allogenic control. Small-scale interactions resulted from interdunal flooding during periods of erg activity.	20 m on average	Herries, 1993; Hassan et al., 2018; Priddy and Clarke, 2020
The Upper Jurassic	Fluvial channels,	The vertical transition from fluvial to aeolian	~4–18 m	Veiga and

Quebrada del Sapo Formation, Neuquén Basin, Argentina	sheetfloods, distal ephemeral fluvial systems, aeolian dunes, aeolian sandsheets and dry and wet interdunes.	deposits reflected a local climatic change or a lowering of the water table during periods of low sea level.		Spalletti, 2007; Spalletti and Veiga, 2007
The Lower Cretaceous Twyfelfontein Formation, Huab Basin, northwest Namibia	Ephemeral fluvial channels, sheetfloods, aeolian dunes, aeolian sandsheets and dry and damp interdunes.	The drying-wetting cycles developed. The vertical transition from ephemeral fluvial to aeolian units recorded climate or subsidence controlled fluctuations on the groundwater level relative to the depositional surface.	5–10 m	Mountney et al., 1998, 1999
The Upper Cretaceous Candeleros Formation, Neuquén Basin, Argentina	Aeolian dunes, wet interdunes, channelized and non-channelized fluvial deposits	The vertical fluvial–aeolian interaction units represent the contraction/expansion of an erg-margin system as a result of variations of the water table position to climatic conditions.	~2–21 m	Mayoral et al., 2021
The Upper CretaceousBarun Goyot Formation, Gobi Basin, Mongolia	Aeolian dunes, wet interdunes, intermittent streams,	The succession was deposited under conditions of hot and semi-arid climate. The drying-wetting cycles recorded climate controlled variations in the water level.		Gradzinskiand Jerzykiewicz, 1974
The Upper Cretaceous Daijiaping Formation, Chaling Basin, China	Aeolian dunes, aeolian sandsheets, damp and wet interdunes, bedload streamflows, fluvial channels, sheetfloods and floodplains.	The distinct fluvial–aeolian interaction system was recognized. The wetting-upwards cycles developed. The vertical stacking of fluvial and aeolian deposits bounded by erosive supersurfaces reflected the contraction and expansion of erg-margin systems in response to climate changes.	0.4–14.2 m	This study

1552

1553